Frequency dependence of an alternating magnetic field driven flow

Marco Zennaro

CONTENTS

LIST OF FIGURES

List of Figures

ABSTRACT

The flow driven by a single phase alternating magnetic field (AMF) in an electrical conducting fluid is studied experimentally. Flow measurements were carried out with an ultrasonic Doppler velocimeter. The project SIKELOR, funded by the European Commission, has been supporting researches on the purification of silicon melt from electrical non-conducting impurity particles, *via* Leenov-Kolin force (LKF). This electro-phoretic force can be produced applying an AMF. Since any flow strongly interacts with the LKF-driven separation, in particular the AMF-driven flow deserves a detailed investigation. The present research shows that the difference of flow patterns as frequency changes is greater than expected, questioning the validity of previous results on the dependence of flow structure on frequency. Maximum flow velocities, around 3 mm/s, suggest a laminar regime; however remarkable oscillations of kinetic energy were observed, not attributable to harmonic oscillations. The measurements could be fairly reproduced by a numerical simulation, the knowledge of the entire flow field of which brings about a better insight into the complex phenomena in AMF-driven flows.

ABSTRACT

INTRODUCTION

1.1 BACKGROUND

The use of magnetic fields in metallurgical industry is widespread throughout several applications, such as casting, stirring, heating and levitation. In 1819 Faraday began his researches on alloy steel [1]; unfortunately due to the limited knowledge of metallurgy of his contemporaries and the insufficiency of industrial competences the intuitions of Faraday could not be implemented[1]. Only a few decades later, following Heaviside's and Thompson's studies [3, 4] regarding Joulean heating and eddy currents, in 1871 de Ferranti was able to design the first induction heating furnace [5], which however worked only at low frequencies. In 1919, Northrup commenced studies on induction furnaces aiming at a higher range, i.e. 20-80 kHz [6].

The needs of metallurgical industry generated a deal of enhancements and the effectiveness of induction furnaces was substantially improved. Thus, in the sixties of the previous century the technology was commonly considered mature. However in the following years a demand emerging from new technologies, such as continuous casting, combined with the influence of the energy crisis, led to a new revival of researches. It was the upcoming branch of metallurgical Magnetohydrodynamics (MHD) which distinctly contributed to this restage of work [2, 7]. Even though this branch of science could explain many phenomena and improve many metallurgical processes, not everything has been cleared [2]. Among the still controversially discussed issues, the estimate of stirring velocities inside a furnace plays a key-role. Further experimental investigation is needed.

In induction heating furnaces, an alternating magnetic field (AMF) produced by an alternating current circulating in a coil induces an eddy current J in the melt. The desired heating is established by Joule dissipation J^2/σ, where σ is the electrical conductivity. In addition, the interaction between J and the AMF that induced it leads to an electromagnetic force. This Lorentz force may drive a flow inside the melt, which is often desirably since it can provide an effective stirring.

To understand how stirring is initiated, consider as an example a cylinder whose height is significantly larger that the base radius, such that border effects can be neglected in the central region. A system of coils, oriented parallel to the cylinder axis, surrounds the cylinder. Lorentz force $\mathbf{F} = \mathbf{J} \times \mathbf{B}$, where $\mathbf{B}$ is the magnetic induction and $\mathbf{J}$ is the induced current density, must be calculated to assay how stirring comes out. The magnetic induction field generated by the coils is $\mathbf{B} = (B_r, 0, B_z)$ and it is commonly assumed $B_r \ll B_z$. $\mathbf{J}$ circulates in the ϕ direction. Thus $\mathbf{F}$ is directed along the radial component: it can be easily seen that $\nabla \times \mathbf{F} = 0$. A sketch of the convective pattern is represented in figure 1.

---

1 These experiments of Faraday assign to this great scientist the title of father of Magnetohydrodynamics, see Davidson [2].
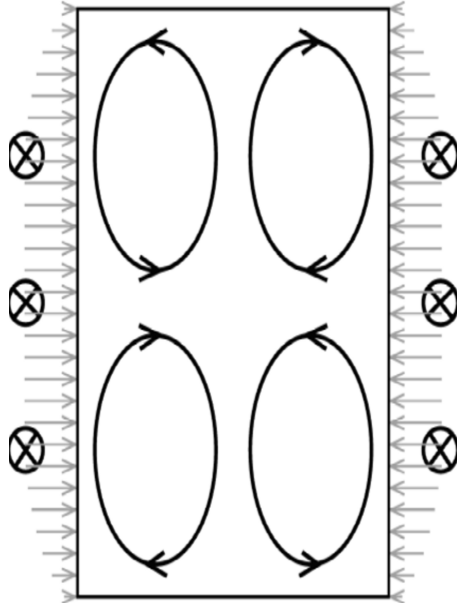
Figure 1: Sketch of the double-toroidal flow structure driven by an alternating magnetic field (AMF). The windings of the coil are indicated by a circle with an "X" inside, extending vertically less than the fluid's height. Grey arrows represent the major component of the magnetic field B_z decreasing towards the top and the bottom due to the end effect of a short coil. As the electric current J induced inside the electrically conducting fluid circulates mainly in the azimuthal direction, the corresponding Lorentz force is in the radial direction. I.e., the majority produces a pressure.

The component B_z of the magnetic induction field decreases to the end of the axis, therefore the induced $\mathbf{J}$ decreases and the radial force faces a quadratic decrease; this can be seen *via* the grey arrows in figure 1, which become shorter at the top and the bottom of the container. Supposing that the B_r component could be neglected even when the component B_z decreases, then it is the axial variation of the radial force which creates the curl of F ; the force, being stronger in the middle of the axis, pushes the fluid inwards, causing a circulation of the fluid to the top and the bottom of the container and then again inwards to the horizontal axis. The flow structure originated from those physical phenomena is commonly called double-loop structure.

As far as consequences for induction furnaces are concerned, as Tarapore & Evans, Davidson and Lupi pointed out two clear advantages are obtained, i.e. melt homogenization and heat transport from the boundaries to the melt core, while on the other hand stirring causes erosion of vessel refractories [2, 8, 9].

Due to skin effect, the modulus of the magnetic induction field $\mathbf{B}$ tends to be higher on corners, therefore just a small part of the melt sets the entire flow; as noted by Davidson , the flow can be controlled just by small changing of $\mathbf{B}$ [2]. Electromagnetic forces are determined by different parameters, such as furnace geometry, frequency and coil position; the force distribution, as noted by Davidson et al. [64], is confined to a small corner region near the coils and $\nabla \times \mathbf{F}$ is almost negligible outside this region. Frequency can change the amplitude and the spatial distribution of Lorentz forces for a fluid magnetically driven, according to [10, 11]; frequency has also an effect on the shear layer and on turbulence characteristics. Thus an inquiry into the influence of this parameter over the behaviour of a specific fluid turns out to be fundamental.

One of the first experimental confirmations of the well-believed double-loop structure was provided by Grandjean [12]: investigating mercury flow patterns by a plate immersed in the melt of a core-less induction furnace, with a diameter of $300 \; mm$ and frequency f $50 \; Hz$, he found out a double-toroidal structure for $S \approx 9$, where S is the shielding parameter

$$S = \mu \sigma \omega R^2 \qquad (1)$$

This parameter indicates the distribution of current according to the skin effect, with $\omega = 2\pi f$, while μ and σ are the magnetic permeability and the electrical conductivity, respectively.

Following the theoretical works of Damaskos and MacAnlis on frequency f [13, 14], Bednarz carried flow measurements in a mercury induction furnace to verify these predictions [15]. After he had built a device to find out the direction of the flow within the furnace, he estimated the position with the strongest flow by $\frac{r}{R} = 0.63$: comparing his measurement with the calculations of MacAnlis for $S = 10$, he observed that this point was quite in agreement with theoretical predictions performed in [13, 14]. Therefore he argued that this position could be representative to measure the characteristic velocity v_c, defined as the velocity which can describe the flow motion within the fluid. Measurements were carried out by Bednarz with constant power and constant stirring for several S. Since remarkable oscillations of fluid flow were detected by the probe, Bednarz proposed a model to explain why these oscillations appeared: according to the author, the interaction of the double toroidal pattern with the walls of the furnace, composed by two main eddies, caused a shear flow which generated unstable secondary toroids. Thanks to the noteworthy work of Bednarz it was suggested the interesting idea that the double toroidal structure is not fixed in time and that the double toroidal model is too simplified to correctly describe the fluid flow.

Even if some new results were achieved with this experimental setup not all the questions were answered, neither it would have been reasonable to expect a full description of the flow of a core-less furnace given the approximations in modeling the apparatus and the limitations in the experimental techniques.

For example, is it really acceptable to consider only one component of velocity as adequate to describe the fluid flow? May it be too rushed to consider the average velocity along the z axis $\langle v_z \rangle$ the so-called characteristic velocity? Lastly, the model proposed for the eddies modifications could be applicable for rather different S, say 20 or 100?

Tarapore & Evans developed a predictive model for fluid flow and compared their computations with measurements conducted on a mercury pool, with an induction system provided by a Tocco 30 Kw, 3 KHz induction furnace power supply; the measurements were carried out with a stroboscope [8]. The shielding parameter was quite high, $S \approx 514$. Comparisons were made for different coil current levels and for different geometries; the double-torus structure seemed confirmed both theoretically and experimentally and one of the two vortices was bigger than the other when the coil system was put upwards or downwards the melt.

In 1980 Hunt & Maxey estimated the mean and the turbulent velocity in a induction furnace, taking also into account the shear stresses [16]. Balancing the electromagnetic and shear stress terms, for mean velocity (near the wall) they found:

$$\overline{v_0} \approx \left(\frac{\delta}{L}\right)^{\frac{1}{2}} * (v_a) \tag{2}$$

where v_a is the Alfvén speed, defined as

$$v_a = \frac{B}{\sqrt{\mu\rho}} \tag{3}$$

Hunt & Maxey estimated the core velocity $\overline{U}_{core}$ by continuity:

$$\overline{v}_{core} \approx \overline{v}_0 2\frac{\delta_T}{R} \tag{4}$$

where R is the furnace radius and δ_T is the thickness of side layers diffusion into the melt, caused by turbulence. In regard to fluctuating velocity, the authors gave this estimate

$$\frac{\widetilde{v_0}}{\overline{v_0}} \approx \frac{\overline{v_0}}{\omega\delta} \tag{5}$$

Therefore, following this expression, for high enough frequencies the fluctuating velocity is small, whereas for low frequencies the fluctuating component of velocity can be compared to the mean one.

As far as laminar flow is concerned Moreau argued that in this case the mean velocity could be estimated thanks to a balance between inertial forces and the mean stirring force [17]. Moreover the author summarized the criteria which should have led to a prediction of the flow regime, at least for the laminar case. First of all, according to the author, the shielding parameter S set the configuration of the flow regime and separation theory was indicated as the correct tool to predict the size and the number of vortexes . Secondly, the velocity scale was determined by the electrical current in the coil or by the external magnetic field. Eventually Moreau noted also that it was still not clear whether those results could have been acceptable also in turbulent regime, quoting as an example recirculating turbulent flows in cavities [17].

Moore & Hunt were the first to measure the mean velocity field and the fluctuating velocity in an induction furnace filled with mercury, working at frequency $f = 50Hz$ [18]; they found out a double-toroidal structure and the peak of velocity near the wall. The velocity was proportionally to magnetic field intensity. These results were later found in good agreement with the theoretical predictions.

Trakas et al. carried out an experimental study in an induction furnace filled with mercury, in a range within $2,7 < S < 17,8$; an hot-film anemometer was used to measure velocity [19]. The authors noted how the coil current intensity had no influence on the flow structure, whereas the structure was influenced by frequency. Furthermore, the authors showed how the velocity, both in the case of surface melt measurements and other flow points, was clearly directly proportional to coil current, in agreement with [18, 21]. Then Trakas et al. provided the variations of maximum velocity value near the crucible wall as a frequency of S: the velocity increased rapidly, but at the same time there was a saturation of S for $S \approx 18$. This initial increase was found consistent to a relation proposed in other works [15, 17], i.e. $V_{\mathrm{max}} \approx S^{\frac{1}{2}}$. Eventually it seemed not clear, whether this saturation could exist even for higher S, because, as the authors argued, there was neither experimental nor theoretical evidence of it.

Later Taberlet & Fautrelle carried out a new experimental study in an induction furnace filled with mercury, with a directional probe and an hot film-anemometer: they aimed to investigate the influence of frequency in a larger range of S [20]. This range was set by the ratio $\frac{\delta}{a}$, where δ is the skin depth and a the furnace's radius: the maximum value and the minimum value of $\frac{\delta}{a}$ were 0.7 and 0.07, correspondent to a frequency range of $50 - 5000Hz$. As far as the mean flow is concerned Taberlet & Fautrelle confirmed that the coil current had no influence, as was previously stated [19, 22]. Measuring the flow patterns, by $S = 3.9, 30, 166, 372$, the authors observed the typical double toroidal structure for all the cases, except for $S = 166$, where three eddies were detected: even though the authors stressed the difficulty in giving an interpretation of the flow structure, it seemed clear that it depended only on the frequency. The velocity profile was again found in linear relationship with the coil current; in regards to the relationship between velocity profile and frequency, the maximum of velocity was found near the wall, even though the precise position could not specified, due to a lack of accuracy previously stated by Taberlet & Fautrelle: a maximum of velocity was found for $S \approx 40$. So it was experimentally confirmed the existence of a region with a maximum of stirring velocities, in agreement with other studies [8, 22]. For larger S, the author found reasonable the relation $v \propto S^{-\frac{1}{4}}$ proposed before by different authors [22, 23].

El-Kaddah & Skezely carried out an experimental and a numerical study with the same experimental set up used by Taberlet & Fautrelle [24]: the double-toroidal structure was confirmed both by measurements and computations, but for the case $S = 166$ there was a discrepancy between the numerical computation and the measurements, because four loops were measured, whereas the calculated pattern presented two loops; however it was not clear to the authors whether this disagreement could be caused by the numerical model or by the known uncertainties due to these kind of experiments.

Therefore, reviewing all these results it seems that the flow structure made of two recirculating loops can be considered confirmed, this evidence being also confirmed by subsequent studies (Galpin & Fautrelle 1992 Stelian et al. 2006 Hamaki et al. 2011).

Such deal of studies, which would lead to consider the double toroidal pattern confirmed, arise the question whether it is necessary to carry on new experiments on the subject. However, a new interest studying flows due to induction heating has been stimulated from the branch production of solar silicon. The process of slicing silicon into cast causes a loss of material reaching the 50 % of the original material, a waste which is no longer endurable.

In 2010 Dughiero et al. proposed a new crystallization furnace, based on induction heating, in place of traditional resistance heating [28]. According to the authors, replacing resistors with an induction mechanism guarantees a reduction of heating and melting times. A previous study by the same authors, based on numerical simulations, had already shown how energy and time could have been saved in percentage up to 20 % [29].

Owing to the innovative system described in [28], a project within the Framework Programme 7 of the European Commission was developed and launched, named SIKELOR [30], aiming to use the furnace proposed by Dughiero et al. to process the silicon waste, in order to obtain a resource-friendly method to reuse the waste and to offer a feedstock which could be competitive with virgin feedstock.

The goal to purify the silicon melt should be reached cleaning the silicon melt *via* electromagnetic processing of materials (EPM): Leenov-Kolin forces (LKF) would be applied to confine non conductive particles at the borders of the melt, so that they could be easily removed [31, 32]. A simple estimate of LKF is provided by Makarov et al. [33]:

$$\mathbf{F}_{\mathrm{L}} = \frac{\delta \omega \sigma B^2}{4} \exp\left(-2\frac{L-r}{\delta}\right) \tag{6}$$

Therefore LKF strongly depends on the frequency of the applied magnetic field; to the best of our knowledge LKF were applied successfully to remove impurities respectively by Taniguchi et al. for aluminium melt [34] and for silicon melt by Kadkhobaeigi et al. [35]. However, not everything has been cleared. A too low frequency would inhibit LKF, whereas a too high frequency would drag off the particles from the wall, that is fluid dynamics forces would overcome electromagnetic separation forces. Being the LKF applied via an AMF, one is concerned with the type of flow created by this kind of magnetic field; therefore a deeper inquiry on the influence of frequency on flow structure is needed.

To prove the necessity of new inquiries Cramer & Galindo conducted an experiment and a numerical simulation to study on which parameters the global flow structure depends on [36]. In particular, they have shown a dependence of the global flow structure on the AMF frequency f. As it can be seen in Fig. 2, there is a maximum for $S \approx 30$. Given that the magnetic field $\mathbf{B}$ is kept constant, it turns out the velocity depends just on frequency. They also presented an analysis of the correlation between Lorentz force and flow structure, which allowed to plot the velocity vector in fig. 3. It clearly turned out that a change of velocity vortices appears near the maximum, as it can be seen in fig. 3; instead of two vortices there are four vortices one on top of another. Furthermore, presenting a time series of the component v_{z}, Cramer & Galindo showed how the vortices are created and destroyed; therefore the well-believed flow structure is not stable and it can be considered just a long-term average structure.

Notably a flow structure made of four vortices was previously found in a numerical computation concerning a flow driven by an AMF in a rotating cylinder [37, 38]: this topology is due to the non uniform distribution of the magnetic field to the corners of the cylinder.

shielding parameter
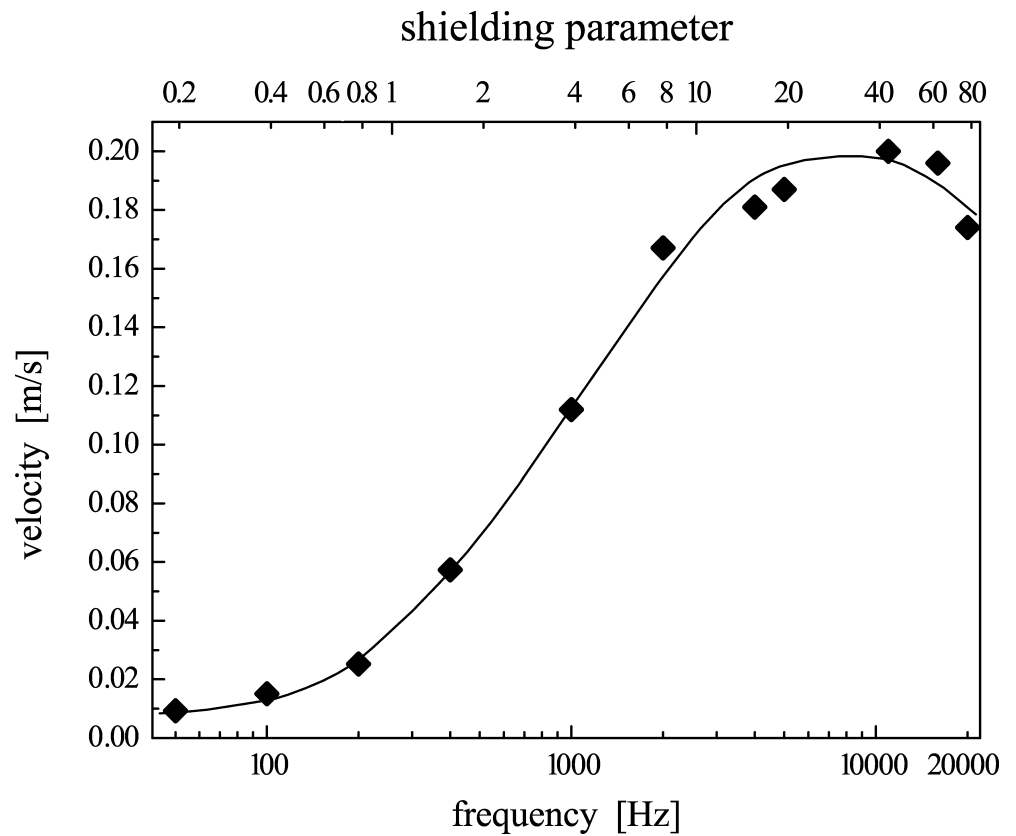
Figure 2: Dependence of velocity on frequency and shielding parameter S. The field **B** is kept constant. The existence of a region with maximum of stirring velocities is again proved, in accordance to previous studies.
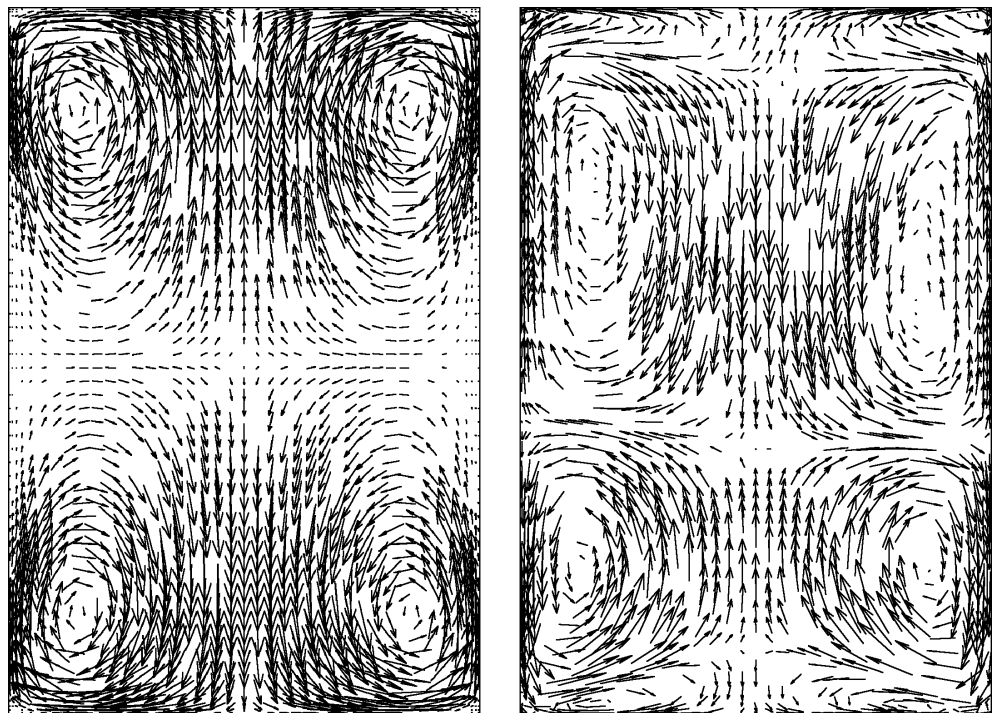
Figure 3: Plot of velocity vectors for 50 Hz (left) and for 11 kHz (right). The figure on the right shows that the flow structure modifies as the frequency changes, i.e. the flow structure is not more composed only by two toroids one on top of another.

Reviewing all these results some questions naturally arise [39, 40]:

- Is really the double toroidal structure the only structure reasonable in induction furnaces?

- Could it be considered just as long-term averaged structure?

- For which value of the shielding parameter could it be considered correct?

- What happens when the frequency increase?

The aim of the present thesis is to propose experimental elements to answer these questions. An experimental study was carried out to investigate the temporal evolution of a fluid driven by an AMF, varying frequencies at fixed current.

2

BACKGROUND

To understand the physics of induction furnaces one is concerned with phenomena coming from different branches of physics, that is electromagnetism, fluid dynamics and heat transfer: in addition, to design a furnace, one is needed to deal into the field of material science. However, being this experiment just a step before the applications of LKF to induction furnaces, problems concerning material science could easily be neglected: furthermore, being the experiment carried out at room temperature, analysis of heat transfer could be dropped out as well.

Scientists and technicians coming from metallurgical MHD have been taking a lot of efforts to clarify the phenomena occurring in an induction furnaces, especially to give an estimate of stirring velocities. Even though not everything has been understood, nowadays it is possible to find this subject treated in different textbooks, i.e. [2, 41]; thus one finds in a concise and elegant way all the equations needed to to comprehend the fundamental laws. The undeniable advantage of MHD is that it allows to describe the physical laws *via* an unified approach; therefore it seems convenient to follow this approach to briefly recall the physical background of induction furnaces.

2.1 REDUCED MAXWELL'S EQUATIONS

Maxwell's equations allow to describe all the laws of electromagnetism in a way which is concise, elegant and precise; however it will be here shown that, as far as MHD is concerned, some assumptions can be done which quite simplify these equations. It can be anticipated that all of electromagnetism which is needed by MHD refers to how electromagnetism was known before Maxwell's work: the equations will be therefore called 'pre-Maxwell equations'. Therefore we start here with Maxwell's equation as they are nowadays known [42]:

$$\nabla \cdot \mathbf{E} = \frac{\rho}{\epsilon_0} \tag{7}$$

$$\nabla \times \mathbf{E} = -\frac{\partial \mathbf{B}}{\partial t} \tag{8}$$

$$\nabla \cdot \mathbf{B} = 0 \tag{9}$$

$$\nabla \times \mathbf{B} = \mu_0 \mathbf{J} + \frac{1}{c^2} \frac{\partial \mathbf{E}}{\partial t} \tag{10}$$

To these relations must be added the conservation charge law and the force law:

$$\nabla \cdot \mathbf{J} = -\frac{\partial \rho}{\partial t} \tag{11}$$

$$\mathbf{F} = q(\mathbf{E} + \mathbf{v} \times \mathbf{B}) \tag{12}$$

As Davidson pointed out, normally MHD deals with forces on bulks instead of particle charges [2]; thus the force law equation is written in another form bringing to

$$\mathbf{F} = \rho \mathbf{E} + \mathbf{J} \times \mathbf{B} \tag{13}$$

where **F** is a force per unit volume.

Anyway, as it has already been pointed out, some simplifications can be assumed for electromagnetic equations needed in MHD. First of all it is possible to neglect the term of the displacement current from equation (10), since, as shown by Landau et al. [43]

$$\frac{1}{c^2}\left|\frac{\partial \mathbf{E}}{\partial t}\right| \ll |\nabla \times \mathbf{B}| \tag{14}$$

Therefore equation (10) needs to be rewritten

$$\nabla \times \mathbf{B} = \mu_0 \mathbf{J} \tag{15}$$

This hypothesis is known as the 'quasi-steady approximation' [44]: it is acceptable because, as far as MHD is concerned, the condition

$$v \ll c \tag{16}$$

is always verified, i.e. there is no relativistic motion. Dropping out the displacement current modifies the equation of continuity: it becomes in fact

$$\nabla \cdot \mathbf{J} = 0 \tag{17}$$

But one should always pay attention on the frame of reference as Roberts observed [44], because normally Ohm's law

$$\mathbf{J}' = \sigma \mathbf{E}' \tag{18}$$

is applied to a frame of reference integral to the motion of the fluid: $\mathbf{J}'$ and $\mathbf{E}'$ in fact represent the electrical field and the current density in a frame moving with the fluid. Thus one needs to consider the transformation laws, as reported in [45]:

$$\mathbf{E}' = (1 - \gamma_{\mathrm{v}})\frac{(\mathbf{v} \cdot \mathbf{E})}{v^2}\mathbf{v} + \gamma_{\mathrm{v}}(\mathbf{E} + \mathbf{v} \times \mathbf{B}) \tag{19}$$

$$\mathbf{B}' = (1 - \gamma_{\mathrm{v}})\frac{(\mathbf{v} \cdot \mathbf{B})}{v^2}\mathbf{v} + \gamma_{\mathrm{v}}(\mathbf{B} - \frac{\mathbf{v} \times \mathbf{E}}{c^2}) \tag{20}$$

where

$$\gamma_{\mathrm{v}} = \frac{1}{\sqrt{1 - \frac{v^2}{c^2}}} \tag{21}$$

Keeping in mind that one deals with a non relativistic case, it follows

$$\mathbf{E}' = \mathbf{E} + \mathbf{v} \times \mathbf{B} \qquad \mathbf{B}' = \mathbf{B} \qquad \mathbf{J}' = \mathbf{J} \tag{22}$$

Therefore one obtains Ohm's law in the laboratory frame:

$$\mathbf{J} = \sigma(\mathbf{E} + \mathbf{v} \times \mathbf{B}) \tag{23}$$

Another simplification can be done in regards to the force equation, because for the non-relativistic case the electric charge density is almost negligible [44]. Being

$$|\mathbf{E}| \approx \frac{l}{\tau}|\mathbf{B}| \tag{24}$$

where l and τ are the length scale and the time scale of the system respectively, it is readily seen that

$$\frac{|\rho \mathbf{E}|}{|\mathbf{J} \times \mathbf{B}|} \approx \frac{|\nabla \cdot \epsilon \mathbf{E}||\mathbf{E}|}{\left|\nabla \times \frac{\mathbf{B}}{\mu}\right||\mathbf{B}|} \approx \epsilon\mu\left(\left|\frac{\mathbf{E}}{B}\right|\right)^2 \approx \left(\frac{l}{c\tau}\right)^2 \ll 1 \tag{25}$$

therefore the term $\rho\mathbf{E}$ can be dropped out, bringing to

$$\mathbf{F} = \mathbf{J} \times \mathbf{B} \tag{26}$$

The new force equation can be alternatively formulated thanks to tensor notation:

$$
\begin{aligned}
(\mathbf{J} \times \mathbf{B})_i &= \frac{1}{\mu} \epsilon_{ijk} (\nabla \times \mathbf{B})_j B_k \\
&= \frac{1}{\mu} \epsilon_{ijk} \epsilon_{jlm} \frac{\partial B_m}{\partial x_l} B_k \\
&= \frac{1}{\mu} (\delta_{kl} \delta_{lm} - \delta_{km} \delta_{il}) \frac{\partial B_m}{\partial x_l} B_k \\
&= \frac{1}{\mu} B_k \left(\frac{\partial B_i}{\partial x_k} - \frac{\partial B_k}{\partial x_l} \right) \\
&= \frac{\partial}{\partial x_k} \left[\frac{1}{\mu} \left(B_i B_k - \frac{1}{2} B^2 \delta_{ik} \right) \right] \\
&= \frac{\partial m_{ik}}{\partial x_k}
\end{aligned}
\tag{27}
$$

where

$$
m_{ij} = \frac{1}{\mu} \left(B_{ij} - \frac{1}{2} B^2 \delta_{ij} \right)
\tag{28}
$$

The scalar product of (23) with $\mathbf{dS}$ is

$$
\frac{1}{\mu} \mathbf{B} (\mathbf{B} \cdot \mathbf{dS}) - \frac{1}{2\mu} B^2 \mathbf{dS}
\tag{29}
$$

where the second term is called the magnetic pressure.

The equations rearranged and represented in the next table describe electromagnetic phenomena as far as it is concerned MHD. Gauss' Law for electrical field has been dropped out because electric charge density ρ has been neglected.

Equations	
$\nabla \cdot \mathbf{B} = 0$	Gauss' Law
$\nabla \times \mathbf{B} = \mu_0 \mathbf{J}$	Ampere's Law
$\nabla \times \mathbf{E} = -\frac{\partial \mathbf{B}}{\partial t}$	Faraday's Law
$\nabla \cdot \mathbf{J} = 0$	Conservation Charge
$\mathbf{J} = \sigma (\mathbf{E} + \mathbf{v} \times \mathbf{B})$	Ohm's Law
$\mathbf{F} = \mathbf{J} \times \mathbf{B}$	Laplace's Law

2.2 NAVIER-STOKES EQUATIONS FOR MHD

Navier-Stokes equations describe in general term the behaviour of all the fluids, even though the analytical solution of these equations is possible just for a very small group of cases. As far as MHD is concerned, it must be taken into account that this branch of physics deals with an electrically conducting fluid, thus the Laplace force must be inserted in the system of equations.

First of all it seems proper to start with the system of Navier-Stokes equations for incompressible fluids in classical fluid dynamics [46, 47]: using vector notation it follows

$$
\nabla \cdot \mathbf{v} = 0
\tag{30}
$$

$$
\rho \frac{D\mathbf{v}}{Dt} = -\nabla p + \rho g + \mu \nabla^2 \mathbf{v}
\tag{31}
$$

Equation 30 and 31 represent the mass conservation and the momentum conservation respectively. Equation (31) can be written with tensor notation [44]

$$
\rho \frac{Dv_i}{Dt} = \frac{\partial p_{ij}}{\partial x_i} + F_i
\tag{32}
$$

where $\mathbf{F}$ is the body force for unit volume and $p_{ij} = -p\delta_{ij} + \pi_{ij}$. The tensor π_{ij} is defined as the viscous stress tensor for incompressible fluids. The complete expression of this tensor is normally written as [44]

$$\pi_{ij} = \rho(\zeta - \frac{2}{3}\nu)\frac{\partial v_k}{\partial x_k}\delta_{ij} + \rho\nu(\frac{\partial v_i}{\partial x_j} + \frac{\partial v_j}{\partial x_i}) \tag{33}$$

Because of incompressibility condition, the first term in the right member of the equation can be neglected, as it is shown in [46]. Therefore π'_{ij} is defined as

$$\pi'_{ij} = \rho\nu(\frac{\partial v_i}{\partial x_j} + \frac{\partial v_j}{\partial x_i}) \tag{34}$$

The tensor π_{ij} is defined not considering the presence of the magnetic field $\mathbf{B}$, i.e. $\mathbf{B} = 0$. If $\mathbf{B} \neq 0$

$$p_{ij} = -p\delta_{ij} + \pi'_{ij} + m_{ij} \tag{35}$$

Now substituting (34) and (35) in (36) it follows:

$$\rho\frac{D_i}{Dt} = -\frac{\partial P}{\partial x_i} + \frac{\partial}{\partial x_j}[\rho\nu(\frac{\partial v_i}{\partial x_j} + \frac{\partial v_i}{\partial x_j})] + \frac{B_j}{\mu}\frac{\partial B_i}{\partial x_j} + F_i \tag{36}$$

In the case of incompressible fluid density it is known that ρ is constant and it also considered acceptable for fluids to consider ν as a constant. Therefore the last expression can be rewritten as

$$\rho\frac{D_i}{Dt} = -\frac{\partial P}{\partial x_i} + \frac{\partial}{\partial x_j}\rho\nu[(\frac{\partial v_i}{\partial x_j} + \frac{\partial v_j}{\partial x_i})] + \frac{B_j}{\mu}\frac{\partial B_i}{\partial x_j} + F_i \tag{37}$$

This equation can be alternatively reformulated using a form where appears the Lorentz force

$$\rho\frac{D_i}{Dt} = -\frac{\partial P}{\partial x_i} + \frac{\partial}{\partial x_j}\rho\nu[(\frac{\partial v_i}{\partial x_j} + \frac{\partial v_j}{\partial x_i})] + (\mathbf{J} \times \mathbf{B})_i + F_i \tag{38}$$

2.3   A TRANSPORT EQUATION FOR VORTICITY

It is well known that as far as fluid dynamics is concerned, it is often used the vector vorticity $\boldsymbol{\omega}$

$$\nabla \times \mathbf{v} = \boldsymbol{\omega} \tag{39}$$

It has been already said that one here is concerned with the measurements of stirring velocities and that it sounds convenient to take into consideration not the Laplace force but the curl of this force [7]; therefore it is more useful not to analyze velocity but the curl of velocity, vorticity. To understand how vorticity changes within the fluid, one should start again with Navier-Stokes equations

$$\nabla \cdot \mathbf{v} = 0 \tag{40}$$

$$\frac{\partial \mathbf{v}}{\partial t} + (\mathbf{v} \cdot \nabla)\mathbf{v} = -\nabla\frac{p}{\rho} + \nu\nabla^2\mathbf{v} \tag{41}$$

where the term concerning the gravitational force has been neglected for simplicity. According to Davidson [2] this expression can be written as

$$\frac{\partial \mathbf{v}}{\partial t} = \mathbf{v} \times \boldsymbol{\omega} - \nabla(\frac{p}{\rho} + \frac{v^2}{2}) + \nu\nabla^2\mathbf{v} \tag{42}$$

thanks to the vectorial identity

$$\nabla(\frac{v^2}{2}) = (\mathbf{v} \cdot \nabla)\mathbf{v} + \mathbf{v} \times \nabla \times \mathbf{v} = (\mathbf{v} \cdot \nabla)\mathbf{v} + \mathbf{v} \times \boldsymbol{\omega} \tag{43}$$

By applying the definition of vorticity to (42) it follows

$$\frac{\partial \boldsymbol{\omega}}{\partial t} = \nabla \times [\mathbf{v} \times \boldsymbol{\omega}] + \nu \nabla^2 \boldsymbol{\omega} \qquad (44)$$

Being both vectors $\mathbf{v}$ and $\boldsymbol{\omega}$ solenoidal the vectorial identity can be simplified

$$\nabla \times (\mathbf{v} \times \boldsymbol{\omega}) = (\boldsymbol{\omega} \cdot \nabla)\mathbf{v} - (\boldsymbol{\omega} \cdot \nabla)\boldsymbol{\omega} \qquad (45)$$

bringing to write equation (44) in this form

$$\frac{D\boldsymbol{\omega}}{Dt} = (\boldsymbol{\omega} \cdot \nabla)\mathbf{v} + \nu \nabla^2 \boldsymbol{\omega} \qquad (46)$$

The convective derivative $\frac{D}{Dt}(f) = \frac{\partial}{\partial t}(f) + (\mathbf{v} \cdot \nabla)(f)$ tells how the quantity f changes in regards to a specified element of fluid, [2].

Now that the equation expressing the evolution of vorticity has been written, it can be seen how it is composed of two terms, an advection term (first part of the right member) and a diffusion term (second part of the right term). The advection term represents the increase of vorticity due to stretching lines of the field $\mathbf{v}$ [2]. The second term tells that vorticity spreads in the fluid thanks to the viscous term: the diffusion of vorticity presents a behaviour equal to the diffusion of heat in a conductor.

2.4 A TRANSPORT EQUATION FOR B

Ohm's law, Faraday's Law and Ampere's law can be together combined to obtain a relationship between $\mathbf{v}$ and $\mathbf{B}$. In fact

$$\frac{\partial \mathbf{B}}{\partial \mathbf{t}} = -\nabla \times \mathbf{E} = -\nabla \times (\frac{\mathbf{J}}{\sigma} - \mathbf{v} \times \mathbf{B}) = \nabla \times (\mathbf{v} \times \mathbf{B} - \frac{\nabla \times \mathbf{B}}{\mu\sigma}) \qquad (47)$$

Using the vector calculus identity

$$\nabla \times \mathbf{C} = \nabla(\nabla \cdot \mathbf{C}) - \nabla^2 \mathbf{C} \qquad (48)$$

where $\mathbf{C}$ is a general vector field, it follows:

$$\frac{\partial \mathbf{B}}{\partial t} = \nabla \times (\mathbf{v} \times \mathbf{B}) + \lambda \nabla^2 \mathbf{B} \qquad (49)$$

with $\lambda = \frac{1}{(\mu\sigma)^{-1}}$, called magnetic diffusivity. The same equation is written by Moreau in terms of vector potential $\mathbf{A}$ [41], where $\mathbf{B} = \nabla \times \mathbf{A}$

$$\frac{\partial \mathbf{A}}{\partial t} = \mathbf{v} \times \nabla \times \mathbf{A} + \lambda \nabla^2 \mathbf{A}. \qquad (50)$$

The application of (50) is more suitable when one is concerned with applications of alternating magnetic fields.

If one assumes that the fluid is incompressible ($\nabla \cdot \mathbf{v} = 0$) the induction equation for $\mathbf{B}$ can be rewritten

$$\frac{\partial \mathbf{B}}{\partial t} + (\mathbf{v} \cdot \nabla)\mathbf{B}) = (\mathbf{B} \cdot \nabla)\mathbf{v} + \lambda \nabla^2 \mathbf{B} \qquad (51)$$

where the left side of the equation represent the convective derivative $\frac{D}{Dt}$ of the field $\mathbf{B}$; the term $(\mathbf{B} \cdot \nabla)\mathbf{v}$ suggests that the field can be produced by the stretching of the flux lines. Therefore equation (51) shows how the magnetic field is distributed within a conductor and that this distribution is a combination of two different mechanism, that is advection and diffusion.

A dimensionless number can be defined starting from (51),

$$\frac{|\nabla \times \mathbf{v} \times \mathbf{B}|}{|\lambda \nabla^2 \mathbf{B}|} \approx \frac{|\mathbf{v} \times \mathbf{B}|}{|\lambda \nabla \times \mathbf{B}|} \approx \frac{vB}{\lambda \frac{B}{l}} \approx \frac{vB}{l} \qquad (52)$$

where v and l are the characteristic velocity and the characteristic length respectively. In analogy with fluid dynamics this number is usually called the magnetic Reynolds number (Rm)

$$Rm = \frac{vl}{\lambda} = \mu\sigma vl \qquad (53)$$

Thanks to this number, some extreme situations can be easily identified where advection term is much bigger than diffusion and vice versa. When $Rm \gg 1$ equation (51) can be simply reduced to

$$\frac{\partial \mathbf{B}}{\partial t} = \lambda\nabla^2\mathbf{B}. \qquad (54)$$

In this condition there is no convection of the magnetic field: at the limit $Rm \approx 0$ the velocity field $\mathbf{v}$ does not influence the magnetic field, thus the equations governing the fluid (electromagnetic equations and fluid-dynamic equations) can be decoupled, because the fluid can be considered at rest. On the other hand, when $Rm \ll 1$

$$\frac{\partial \mathbf{B}}{\partial t} = \nabla \times (\mathbf{v} \times \mathbf{B}) \qquad (55)$$

Equation (55) is valid for a perfect conductor ($\sigma = \infty$) ; the approximation $Rm \ll 1$ is normally acceptable only on the laboratory scale, while for industrial applications and astrophysical scales it can be assumed $Rm \gg 1$.

2.5 STIRRING FORCE ANALYSIS

As far as the stirring force is concerned, it is normally considered the Laplace force: however, as suggested by Davidson [7], taking into account the curl of this force brings advantages to understand what happens within the fluid. Due to reasons of simplicity the cylindrical axially symmetrical case will be calculated [48]: therefore, using cylindrical coordinates $\mathbf{B}$ and $\mathbf{J}$ can be expressed as

$$\mathbf{B} = (B_r, 0, B_z) \qquad (56)$$

$$\mathbf{J} = (0, J_\phi, 0) \qquad (57)$$

and the electric induced field is related to the azimuthal current density by

$$J_\phi = \sigma E_\phi \qquad (58)$$

It will be here taken into consideration not $\mathbf{B}$, but the vector potential $\mathbf{A}$, as reported in [48]. Being in axial symmetric case it follows

$$\mathbf{A} = (0, A_\phi, 0) \qquad (59)$$

Now the field $\mathbf{B}$ must be calculated to get its expression *via* cylindrical coordinates:

$$\mathbf{B} = \frac{1}{r} \begin{vmatrix} \mathbf{a}_r & r\mathbf{a}_\phi & \mathbf{a}_z \\ \frac{\partial}{\partial r} & 0 & \frac{\partial}{\partial z} \\ 0 & rA_\phi & 0 \end{vmatrix} \qquad (60)$$

The field components B_r and B_z can be written in terms of derivatives of A_ϕ

$$B_r = \frac{1}{r}\frac{\partial}{\partial z}(rA_\phi) \qquad (61)$$

$$B_z = \frac{1}{r}\frac{\partial}{\partial r}(rA_\phi) \qquad (62)$$

and it can be normally assumed that the magnetic potential present a time harmonic form

$$A_\phi = g\cos(\omega t + \beta) \qquad (63)$$

with g and β functions depending on r and z. Recalling Faraday's Law and substituting the expression for the magnetic potential it follows

$$\frac{\partial}{\partial t} \nabla \times \mathbf{A} = -\nabla \times \mathbf{E} \tag{64}$$

It is well known that a generic electric field $\mathbf{E}$ can be written as

$$\mathbf{E} = -\nabla V - \frac{\partial \mathbf{A}}{\partial t} \tag{65}$$

but supposing to consider the scalar potential V constant the current density is

$$J_\phi = \sigma E_\phi = -\sigma \frac{\partial A_\phi}{\partial t} = \sigma g \omega \sin(\omega t + \beta) \tag{66}$$

Replacing the expression for A_ϕ in (61) and (62) it gives

$$B_r = -\frac{\partial g}{\partial z} \cos(\omega t + \beta) + g \frac{\partial \beta}{\partial z} \sin(\omega t + \beta) \tag{67}$$

$$B_r = \frac{1}{r} [g \cos(\omega t + \beta) + r \frac{\partial g}{\partial r} \cos(\omega t + \beta) - r g \frac{\partial \beta}{\partial r} \sin(\omega t + \beta)] \tag{68}$$

The expression of the force in the melt can be obtained by

$$\mathbf{F} = \mathbf{J} \times \mathbf{B} = \frac{1}{r} \begin{vmatrix} \mathbf{a}_r & r\mathbf{a}_\phi & \mathbf{a}_z \\ 0 & J_\phi & 0 \\ B_r & 0 & B_z \end{vmatrix} = \mathbf{a}_r J_\phi B_z - \mathbf{a}_z J_\phi B_r \tag{69}$$

Taking the components of $\mathbf{B}$ just calculated, that is B_r and B_z together with J_ϕ, by substitution of those expressions in (67) the mean electromagnetic force $\mathbf{F}$ is

$$\mathbf{F}_m = (\mathbf{J} \times \mathbf{B})_m = -\frac{1}{2}\sigma g^2 \omega [\mathbf{a}_r \frac{\partial \beta}{\partial r} + \mathbf{a}_z \frac{\partial \beta}{\partial z}] = -\frac{1}{2}\sigma g^2 \omega \nabla \beta \partial z = -\frac{1}{2}\sigma g^2 \omega \nabla \beta \tag{70}$$

whereas the average value of the harmonics disappears. Now it is possible to take the curl of the force just calculated:

$$\nabla \times \mathbf{F}_m = -\frac{1}{2}\sigma \omega \nabla \times (g^2 \nabla \beta) = -\frac{1}{2}\sigma \omega (\nabla g^2 \times \nabla \beta + g^2 \nabla \times \nabla \beta) = \tag{71}$$

$$-\frac{1}{2}\sigma \omega (\nabla g^2 \times \nabla \beta + g^2 \nabla \times \nabla \beta) = \frac{1}{2}\sigma \omega 2g \nabla g \times \nabla \beta \tag{72}$$

The cross product of the vectors is readily calculated:

$$\nabla g \times \nabla \beta = \begin{vmatrix} \mathbf{a}_r & r\mathbf{a}_\phi & \mathbf{a}_z \\ \frac{\partial g}{\partial r} & 0 & \frac{\partial g}{\partial z} \\ \frac{\partial \beta}{\partial r} & 0 & \frac{\partial \beta}{\partial z} \end{vmatrix} = -\mathbf{a}_\beta (\frac{\partial g}{\partial r}\frac{\partial \beta}{\partial z} - \frac{\partial g}{\partial z}\frac{\partial \beta}{\partial r}) \tag{73}$$

and substituting this expression in (71) it turns out

$$|\nabla \times \mathbf{F}_m| = \omega \sigma g (\frac{\partial g}{\partial r}\frac{\partial \beta}{\partial z} - \frac{\partial g}{\partial z}\frac{\partial \beta}{\partial r}) \tag{74}$$

EXPERIMENTAL SET UP

The measurements were carried out in a cylindrical container with Radius $R = 17.9$ cm and height $H = 15$ cm. During the experiment the magnetic field has been kept constant, to allow a study depending just on frequency; the maximal frequency tested was $f = 20$ kHz. The maximal magnetic field was $B \approx 1$ mT. The power supply was a function generator connected to an amplifier , whose characteristics are explained in 3.2. The magnetic field was provided by a coil system made of eight separate coils 3.1 .

An ultrasound Doppler velocimeter (UDV) was used for velocity measurements. For the principle and the applications of an UDV see 3.3. The ultrasonic transducer, mounted on a traversing unit, measured the vertical velocity component v_z. The ultrasonic transducer was in kissing contact with the liquid metal.

In regards to the position of the coil system in respect to the container, the first set of measurements was carried out with the coils being not symmetric to the container, as it can be seen in figure 5; this solution was taken because geometry was not foreseen as a parameter which could change the qualitative behaviour of the fluid and also because the induction furnace which will be used in Sikelor project is not symmetrical to the coils: in a second stage of the experiment it was decided for validation to place the coils in an symmetrical position to the z-axis.

3.1 COIL SYSTEM

Four coil groups, each consisting of two separate coils, were available to produce the alternating magnetic field. Figure 4 shows the assembled arrangement with each of the four groups one on top of another.
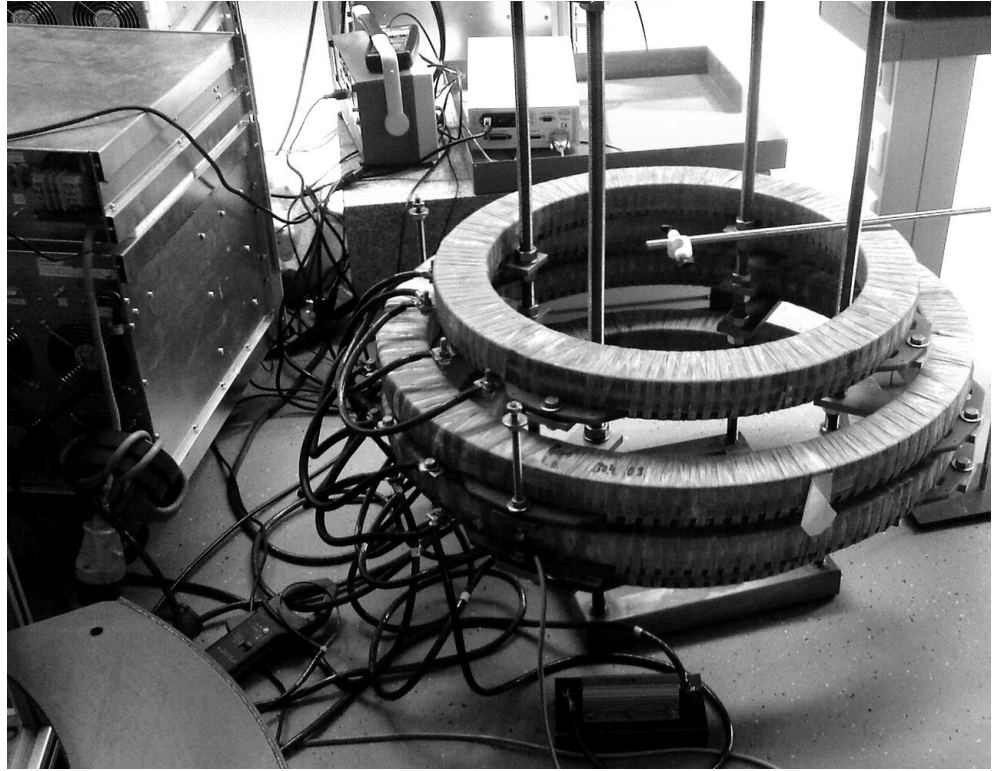
Figure 4: Coil system to produce the alternating magnetic field. Eight separate coils, two of them respectively grouped to what appears as a single coil, with differing numbers of turns and diameters allows a wide range of inductances to be adjusted *via* different wiring schemes.
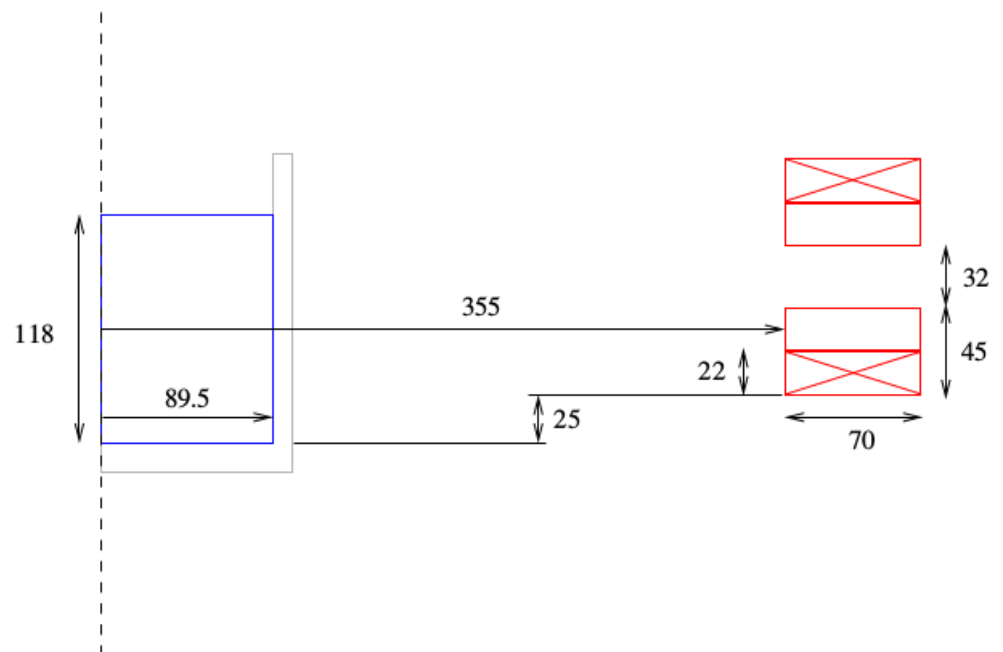

Figure 5: Scheme of the first step of the experiment, carried out with the coils not symmetrical to the container.

The inductance of the four smaller coils was measured as about $L_{SC} = 3.35$ mH. Since this is quite high, they were not used. Owing to the larger diameter and less turns, the inductance of the larger coils is $L_{LC} = 1.125$ mH. For a first test, the horizontally outer with respect to the centre of the system coils of both larger coil

groups was connected in parallel to the power supply. According to the well known inductance L_{tot} of n coils connected in parallel,

$$\frac{1}{L_{tot}} = \frac{1}{\sum_{i=1}^{n} L_i},$$

the inductance of these two coils calculates as $L \approx 0.56$ mH. Mutual inductance were ignored in this rough estimate of L_{tot}. For the maximum planned frequency of $f = 20$ kHz, it is readily seen that the inductive part of the impedance, $\omega L = 70.7$ V/A, exceeds the Ohmic resistance by far. The inductance are further discussed with respect to maximum achievable field strength in conjunction with the maximum ratings of the power supply in Section 3.2.
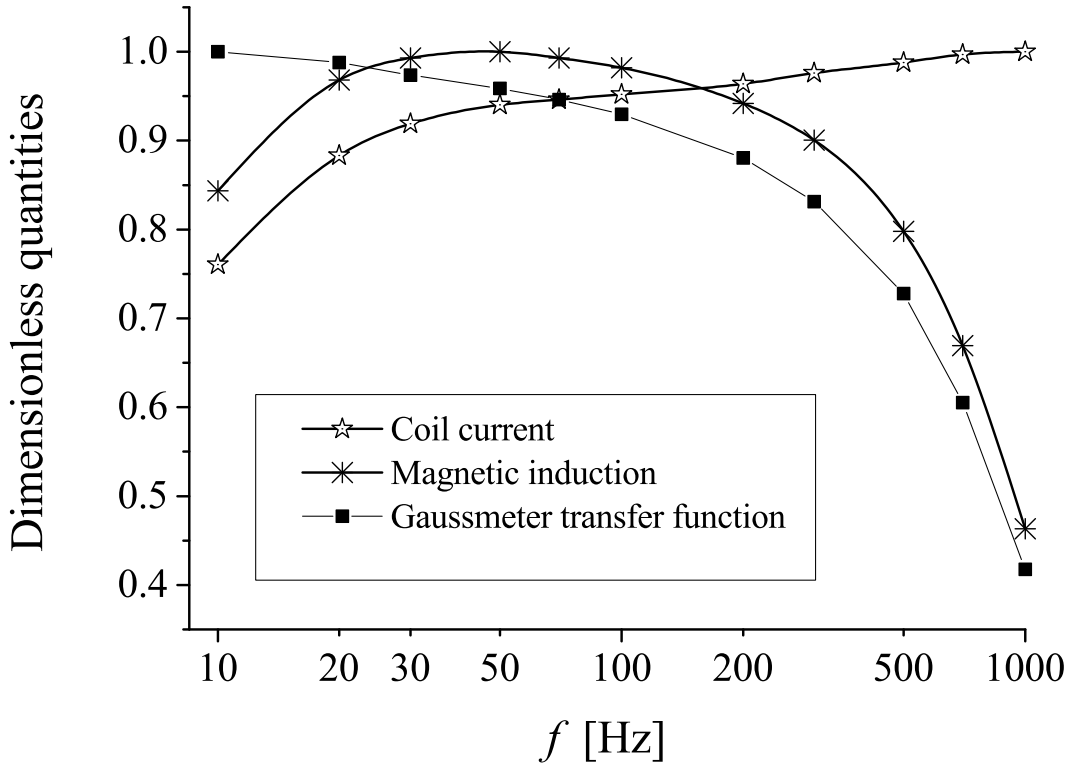

Figure 6: Dependence of the dimensionless current and the magnetic induction on frequency f, with the corresponding transfer function.

3.2 POWER SUPPLY

The core component of the power supply was a HERO® POWER amplifier (model PFL-2250-28 from Rohrer Mess- & Systemtechnik, Munich, Germany) specified with maximum current and voltage output ratings of ± 415 V and ± 28 A. Another component was an Agilent 33220, a function generator providing a wave function [50]. Because of safety reason, a protection with a magnetic relay was installed too. Owing to the high impedance of the coil system, the actually achievable current at higher frequencies was limited. According to Section 3.1, the impedance of the coil system was about 70 V/A, at a frequency of $f = 20$ kHz. Note that the ohmic resistance $R \ll \omega L$ was neglected; it was in the range of mΩ. The 20 kHz were pursued as the minimum upper end of the frequency range for the flow measurements, to ensure that the peak velocity for constant current stirring falls into this range. According to Ohm's law, the maximum current should have been $I_{max} = 4.15$ A$_{eff}$. Actually, it was possible to attain an I_{max} of about 2.6 A$_{eff}$, only. This fact may be explained by (i) the actual inductance of the coils is a little higher than measured and (ii) there is some mutual inductance. In addition, the constant current control circuit of the amplifier caused the safety circuit to switch off before reaching the maximum output voltage. The latter effect is the more pronounced the higher the frequency. This test was carried out with two and four coils in parallel, respectively; within

metering precision, I_{max} was the same in both cases. This indicates that, as assumed under (ii), the mutual inductance is significant.

3.3 DOP 2000

An ultrasonic Doppler velocimeter, type DOP 2000 from Signal-Processing, Lausanne, Switzerland was used for the flow measurements. This measuring technique was at first applied for medical application. The pioneering work of Takeda successfully proved its feasibility in mercury flow [52]. The principle of operation is based on the emission and reflection of short ultrasonic pulses. A transducer emits a pulse into the fluid, in which small particles acting as scatterers are suspended. These particles may be added, or they are naturally present. It is a long lasting experience that in the GaInSn alloy, which was used also in the present work, a sufficient amount of scatterers consisting of agglomerates of oxides is contained. The echo is received by the same transducer being switched from transmission- to reception-mode shortly after the emission, or by a second transducer. In the majority of commercially available devices, including the DOP 2000, the same transducer is used.

The position of the scattering particle, i.e. the distance from the transducer, is readily available from the time of flight τ between emission and reception if the sound velocity c_s is known:

$$x = \frac{c_s \tau}{2} \tag{75}$$

Velocity is obtained by Doppler shift frequency at that moment:

$$v = \frac{c_s f_d}{2 f_0} \tag{76}$$

where f_d stands for Doppler shift frequency and f_0 stands for basic frequency.
The echo received is expressed as

$$R(t) = A(t) \cos(f_0) + B(t) \cos\left[f_0 + f_d(\tau)\right] \tag{77}$$

Being interested just in the Doppler shift frequency, this echo signal is decomposed and a low pass filter is applied to eliminate basic frequency f_0 component. Noise is eliminated by a high-pass filter with a cut off frequency f_{c_s}. In the end the frequency can be converted to velocity profile (to a detailed explanation the reader is invited to see [52]). The maximum depth which can be measured is determined by the pulse repetition frequency (PRF) [51, 52]: in fact the PRF determines the time for the signal to be emitted and to be received from the transducer. The maximal depth is therefore

$$P_{max} = \frac{c_s}{2 f_{prf}} \tag{78}$$

A limit for maximal velocity comes from Nyquist theorem:

$$v_{max} = \frac{c f_{prf}}{4 f_0} \tag{79}$$

As Takeda pointed out, this technique presents three main advantages [53]:

1. **Spatiotemporal information**: The velocity field is obtained as a function of space and time. Being the information of velocity profile contained along the ultrasonic beam, velocity field turns out to be as a function of time.

2. **Application for opaque liquids**: Due to the fact that UDV can be used also with non invasive methods, it is possible to measure opaque liquids as if they are ordinary liquids.

3. **Practical flow mapping**: It often happens to need a validation of numerical computed codes through an experimental work. With UDV the comparison is direct and it concerns not only the flow pattern, but it is also possible a quantitative comparison; in addition to speed other physical quantities (e.g. stream function) can be compared.

This tool has been proving itself as very powerful for different metal liquid flows: Takeda [54] carried out measurements for mercury, while Brito et al. presented the first application of UDV for liquid gallium, a liquid which often has been used for magnetohydrodynamics [56]; Eckert et al. proved his feasibility for liquid sodium [57] and investigation on complex flux structures (InGaSn and mercury) with this technique was performed by Cramer et al. [59]. Anyway, as it is pointed out in [58] and [59] a few questions arise for UDV application to liquid metals :

- Not-performing transducer feasibility at high temperatures.

- Acoustic coupling between interfaces.

- Allocation of reflecting particles.

Solutions for temperature problems are presented by many authors [60, 61]; anyway, considering that the present experiment was carried out at room temperature, this problem was negligible. Regarding acoustic coupling, it should be underlined the necessity of a good wetting contact between the liquid metal and the transducer to guarantee a correct signal transmission, otherwise there could be a change in the acoustic impedance. Furthermore, with progressing time, as Brito et al. observed, there is a continuous deterioration of the signal quality [56]: this phenomenon comes out from the development of oxide layer near the transducer, which makes measurements impossible. Therefore in this case a new wetting contact between transducer and liquid metal has to be established (for oxide layers problem see also [57]).

As it was previously told, a requirement for UDV technique is the presence of tiny particles reflecting back the signal to the transducer. It seems like there is a scarcity of studies regarding signal dependence on various factors, for example particles concentration and morphology, which could improve the measurements. As it is reported in [58], a low concentration causes a deterioration of sensitivity, while an higher concentration, though enhancing the sensitivity, can increase signal attenuation. Thus it is better to work only with impurities present in metals, because adding particles can bring unwanted effects, e.g. agglomeration effects. As far as noble liquid metals are concerned natural tracers are not enough to cause a scattering effect, whereas in gallium alloys oxidation turns out to be unavoidable; in regards to InGaSn, the high oxidation rate in the present experiment had always been a factor to be taken care of (e.g. covering the liquid container with a lid), in order to avoid bad signal quality.

3.4 PROCEDURE

During the first step of this experiment, the test step, it was not clear whether it would have been possible to measure effectively the low fluid velocities expected for such low currents, especially when the frequency was supposed to reach the upper limit of 20 kHz. Thus, a diminution of the upper limit turned out to be necessary; as a maximum was chosen $S = 200$, frequency 960 Hz, expected as a reasonable limit within LKF could have been later successfully applied. Note that this choice would have allowed to the present experiment to be comparable to the most of the studies nowadays available. As minimum limit was chosen $S = 2.5$, because of the current amplifier, not capable to support low frequency.

After various attempts, the chosen current was 9.15 A, corresponding to a magnetic induction B of 0.62 mT: this current value was expected as reachable in the chosen frequency range. Thanks to the magnetic field, the Alfvén $u_a = \frac{B}{\sqrt{\mu\rho}}$ velocity is easily calculated; inserting the value of B into this expressions, the velocity results $6.91 mm/s$. Thus, according to a practical rule of MHD, velocity expected should be around the percentage of Alfvén velocity.

In regards to sensor position, owing to the cross-bar unit, it was possible to shift the sensor position: as first position was chosen the border of the container, being the corner of the container the area where the interaction between fluid and magnetic field is obviously stronger. However, using this only recording position would have looked as a trivial repetition of previous experiments: furthermore, the comprehension of the complete motion within the fluid would have resulted as misleading.

Therefore for every shielding parameter the measurements were repeated in the center of the container and for $R/r = 0.5$, respectively.

Obviously the data recorded from DOP 2000 had to be extracted and elaborated. The elaboration of the results was conducted with several software [1], on the hand Origin® to elaborate data, on the other hand Python and Gnuplot to plot data.

The velocity profile and the flow structure in this work are represented *via* contour plots, with time on the x-axis and the 'gates' on the y-axis, where the gates represents the depth of the ultrasonic beam . As far as the y-axis is concerned, one should note that the depth was measured from the top of the container, where the sensor was in kissing contact with the fluid. In addition to the contour plots, it is also presented the evolution of the square value of the velocity component V_z averaged along the height H of the container

$$V_z{}^2 = \frac{1}{H} \int_0^H v_z{}^2 \, dz \tag{80}$$

The evolution computed in this way can be seen as a qualitative indication of intensity and kinetic energy for the flow circulation in the meridian plane; a similar method was previously used for a flow driven by a rotating magnetic field [62].

cross-bar   power amplifier

Figure 7: Picture of the sensor in kissing contact with liquid metal, with the power amplifier and the traverse unit. The traverse unit, opportunely shifted, allows to measure the fluid flow in several radial positions.

---

1 The author of the present work kindly thanks Dr. Joseph Pal who kindly made available his Fortran code to extract DOP data.

EXPERIMENTAL RESULTS

As previously pointed out, the frequency plays a key-role in the distribution of Lorentz force [20, 63]. The results here presented, not only confirm this statement, but interestingly suggest that it is possible to identify different ranges of S for which the distribution of forces brings to a different flow structure. It could have been reasonable to expect that a different field distribution would have led to very different flow patterns. To the best of our knowledge this assumption is scarcely reported in literature.

Considering that the motion within the fluid is driven by the friction with the wall, here will be normally presented the measurements reported at the rim of the container; however, being the flow structure often complicated and hard to understand, even the measurements recorded for different radial position will be made available. Note that a preference was made for the measurements recorded in the case of symmetrical system; since a symmetric Lorentz force distribution leads in most cases to an asymmetrical flow structure, as it has been already pointed out [69] ; therefore, geometrical symmetry was necessary to simplify an already complicated phenomenon. All these results will be discussed in the subsection 4.1.

In addition to the application to Sikelor project, the present research aims to provide a validation of previous experiments in the field: however, unlike other several works, the attentions is focused more on the kinetic energy than on mean velocity. The reason is straightforward: one here is not merely concerned with a measurement of velocity, but with the understanding of the overall motion within the fluid, as S changes. Thus the results presented in section 4.2 report the mean kinetic energy as a function of S. In opposition to the results concerning flow structure, these results seem consistent with previous researches.

4.1 FLOW STRUCTURE

4.1.1 *S<10*

The first subsection describes the lowest shielding parameter measured, $S = 5$ and $S = 10$. With such shielding parameters, one falls already into the category of the high frequency, $S \gg 1$, namely $\delta \ll L$, where L is the characteristic length; thus a field distribution confined to the corner with the creation of a double toroidal pattern is expected.

The first measurement proposed is $S = 5$, recorded at the rim of the container, in figure 8. At this stage, the structure composed by two eddies is clear beyond any doubt. During the first phase of measurement, the spin up phase of the fluid, the size of the vortexes are comparable: thus the schematic representation of figure 1 is absolutely reasonable, at least until $t \approx 500$ s.

After the spin-up appears a remarkable dissimilarity of size between the lower and the upper vortex, the upper (red) vortex being bigger than the other one; Taberlet & Fautrelle observed for $S = 3.9$ an analogous dissimilarity of size between vortices [20], even though an explanation of this fact is not provided by the authors. As far as the present experiment is concerned, it seems reasonable to formulate two hypotheses for this asymmetry: the first one is based on the influence on the system caused by the legs of the supporting device, made of steel, who could have interacted with the electrical induced currents. Another explanation is based on the hypothesis formulated by Tarapore & Evans [8], who argued that the for the upper loop higher

circulation velocities are expected, due to the lesser liquid solid contact area of this loop: thus, the upper vortex should result stronger.

The maximum motion within the fluid is reached during the spin up of the fluid, by $t \approx 500s$; after that, the mean velocity decreases and oscillates. In order to provide a more understandable visualization of these oscillations, the kinetic energy is plotted in figure 9. It is readily seen how the kinetic energy, after the maximum, steps down and slowly oscillates. Therefore, after the spin up phase, the fluid presents inertial oscillations, a behaviour similar to the evolution proved by different authors for RMF (rotating magnetic field) driven fluids [62, 71].
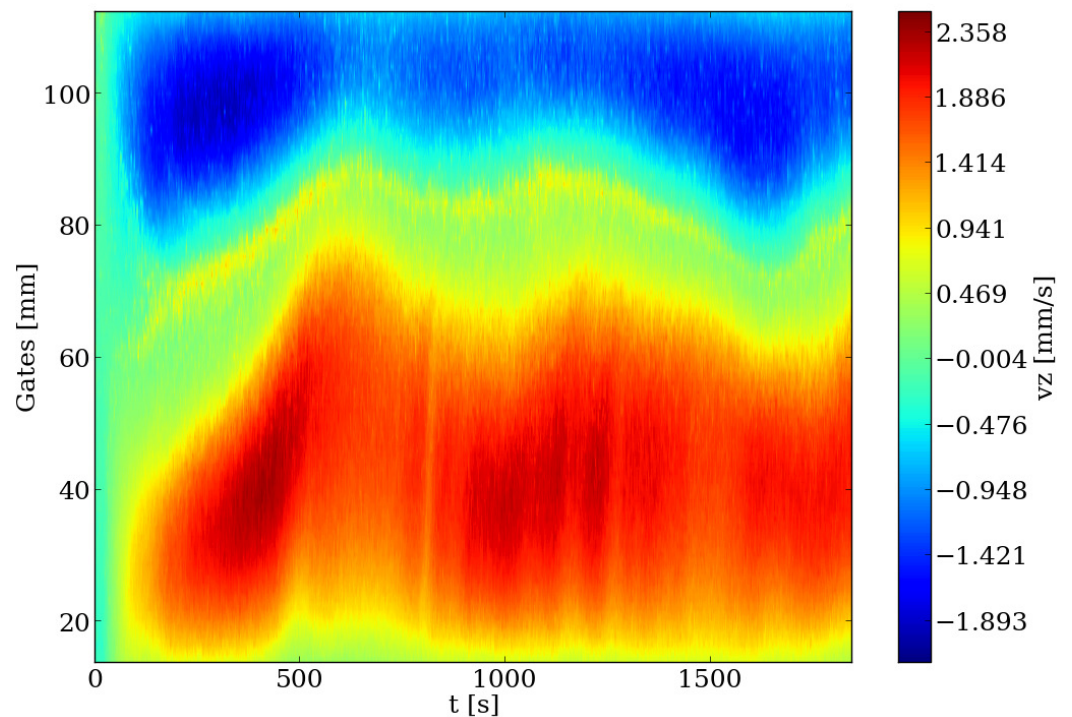
Figure 8: Flow pattern measured at the rim of the container by $S = 5$, corresponding to a frequency of $f \approx 48$ Hz. The scale for the flow pattern is used as a guide, only. Positive velocities, coloured in red, represent regions of downstream, while negative velocities, coloured in blue, represent region of upstream.
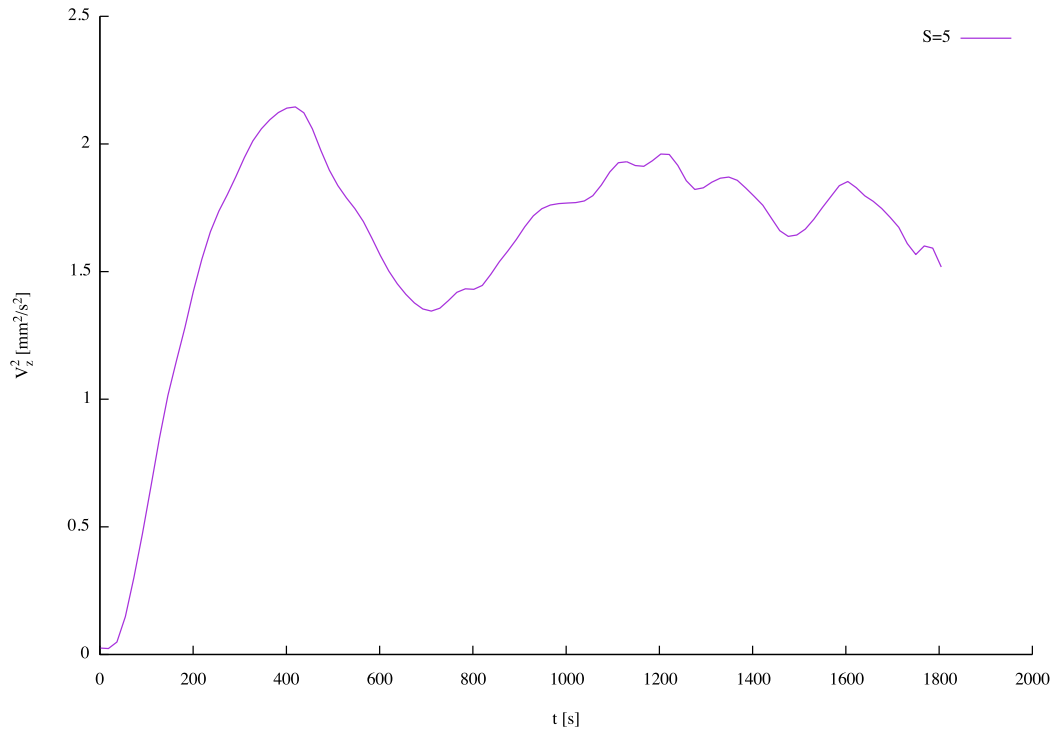
Figure 9: Kinetic energy for $S = 5$ at the rim of the container. A Bezier curve is used as a guide for the eye.

The next shielding parameter value we analyze is $S = 10$, equivalent to a frequency $f \approx 48$ Hz. Quite surprisingly, in this case a deal of observations concerning flow structure and velocity are clear.

In figure 10 it is presented the flow pattern for a measurement carried out at the rim of the container for $S = 10$; in regards to similarities with the precedent case, first of all one sees that, after the spin up of the fluid, the symmetry is 'broken', because the upper vortex is evidently bigger than the lower vortex, although this asymmetry of vortexes is now rather pronounced. The increase of one vortex to the expense of the other one is an observation already noted by Trakas et al. [19]. In analogy to the previous measurement the maximum of velocity appears during the spin up phase of the fluid.

As far as differences are concerned, mean velocities are considerably higher; this observation is consistent with previous studies [15, 19, 24], which show an increase of velocities as the frequency increases. Furthermore, oscillations with a period in order of 10 seconds are noted: at this stage, if one tries to calculate Reynolds number

$$Re = \frac{u_{\mathrm{c}} R}{\nu} \tag{81}$$

the flow is clearly laminar, being $Re \approx 1000$. With some allowance, the maximum velocity is taken as characteristic velocity. The flow regime is laminar, but one can observe velocity oscillations in the order of tens of seconds; this noticeable observation has never been reported in literature.
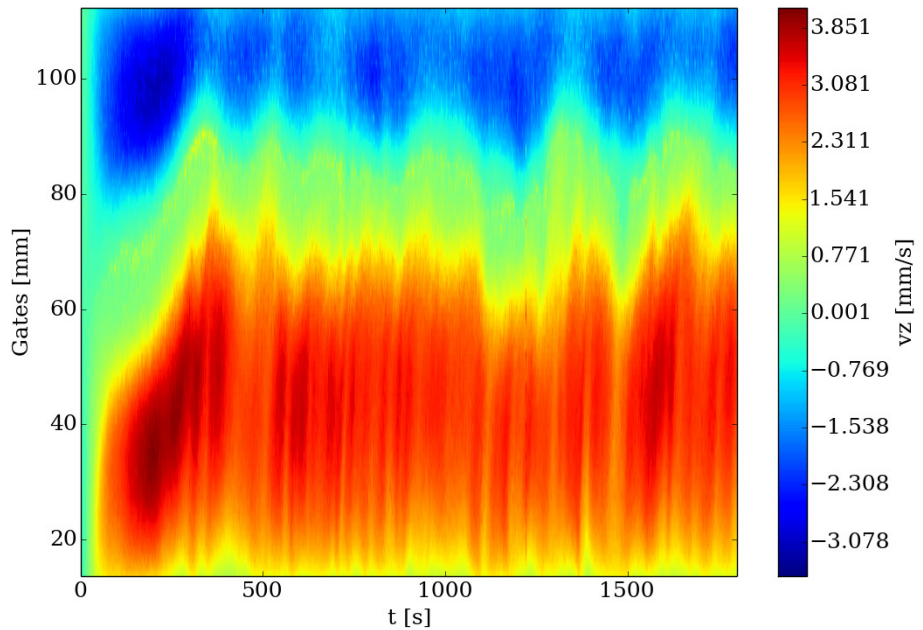
Figure 10: Flow pattern measured at the rim of the container for $S = 10$. The scale for the flow pattern is used as a guide, only. Positive velocities, coloured in red, represent regions of downstream, while negative velocities, coloured in blue, represent region of upstream.

The measurements carried out for lower S indicate a symmetrical structure totally similar to the well-believed double toroidal structure already described. In the work of Galpin & Fautrelle an experiment was conducted in the range $S \in [0.15, 1.48]$; for such a small S the two loops one of top of the another are clear without any doubt [25]: keeping in mind this result and the measurements for $S = 5$ already mentioned, one may suppose that the symmetrical pattern is completely reasonable just for $S < 10$.

To visualize this assumption a comparison of kinetic energy for $S = 5 - 10$ is plotted in 11. The behaviour for these two cases is totally different, because for $S = 5$ oscillations of kinetic energy are not so remarkable and after the maximum is recorded a stationary state is to be found, while for the second case oscillations of kinetic energy are much more remarkable and values of kinetic energy corresponding to less than half of maximum values are recorded. During the spin up phase the kinetic energy for $S = 10$ is more than three times the velocity for $S = 5$: after this phase the kinetic energy for $S = 10$ is always more than double. A modest difference in the shielding parameter frequency leads to very different quantitative and qualitative results.
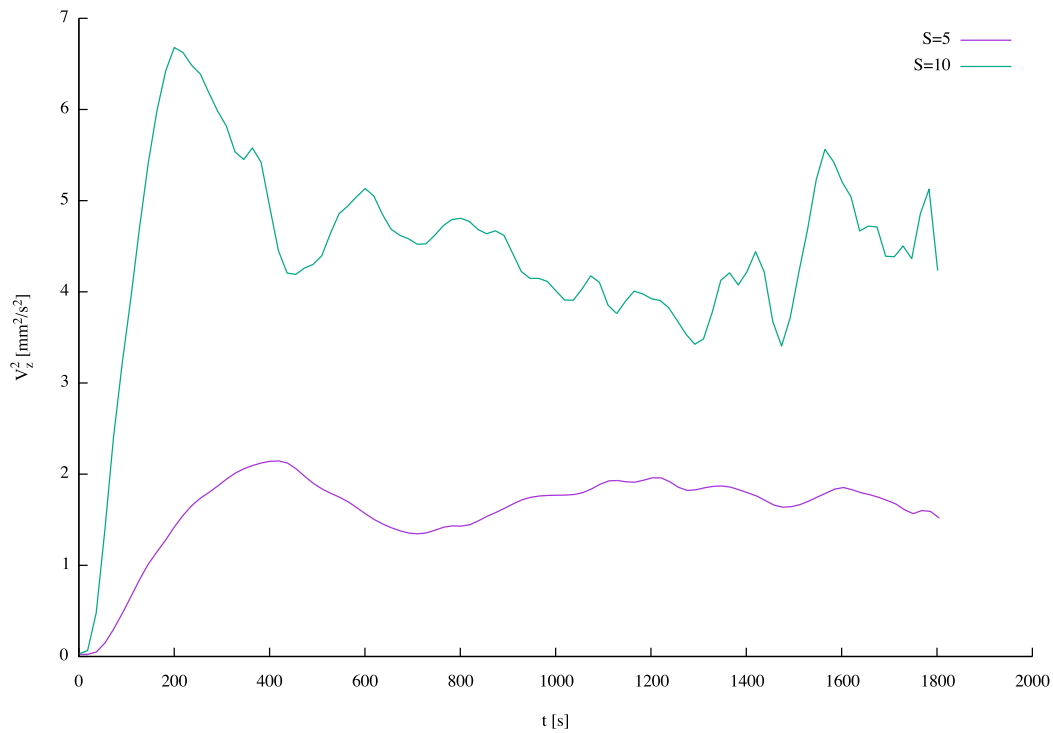
Figure 11: Plot of the kinetic energy at the rim of the container for $S = 5 - 10$. Bezier curves are used as a guide.

As it has just been noted, the flow structure appears not as simple as one may suppose. Therefore, it seems advantageous to present the measurements recorded for $S = 10$ for the positions already mentioned.
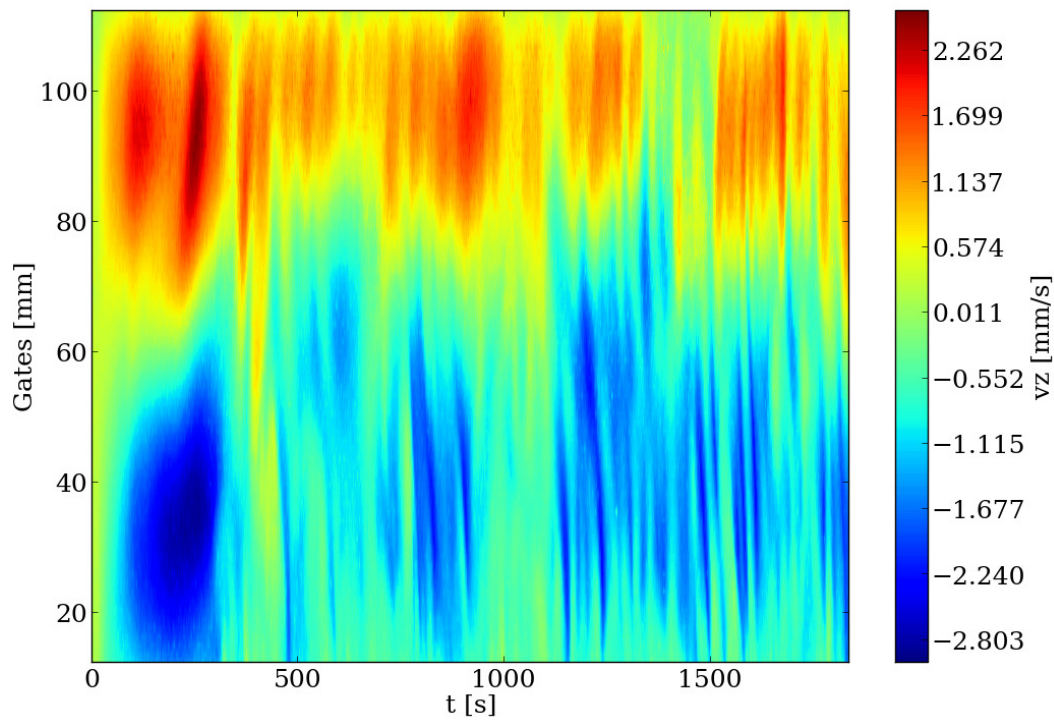

Figure 12: Flow pattern measured at the position $\frac{r}{R} = 0.5$ by $S = 10$. The scale for the flow pattern is used as a guide, only. Positive velocities, coloured in red, represent regions of downstream, while negative velocities, coloured in blue, represent region of upstream.

Being the force concentrated on corners, the most of the fluid is affected by secondary motion; therefore one could imagine that the motion in the fluid in the inner region would be overall similar. As a matter of fact, figures 12 and 13 show interesting similarities and discrepancies with the flow structure plotted in 10.

In regards to similarities, two main common features are noticed: the double toroidal structure during the first phase of the recording time and the fact that the maximum of velocities is recorded during the spin-up. These observations suggest that until $t \approx 450$ s the Lorentz force leads to a symmetrical structure, as one would expect.

Speaking of differences the velocity shows a sharp decrease in the core of the fluid; moreover the structure is much more chaotic and unstable, for example in figure 12, by $t \approx 400$ s the upper vortex expands and the lower vortex gets smaller, while by $t \approx 1400$ s the opposite phenomenon appears. The difference of velocities between the plot recorded at the rim and at $\frac{r}{R} = 0.5$, compared with the differences between $\frac{r}{R} = 0.5$ and the center position, prove how fast the energy decreases into the fluid.

The kinetic energy plotted in figure 15 helps to understand similarities and discrepancies just mentioned: the trend is analogous for the three situations, i.e. strong initial increase and then oscillations, even though there is a remarkable difference in energy.
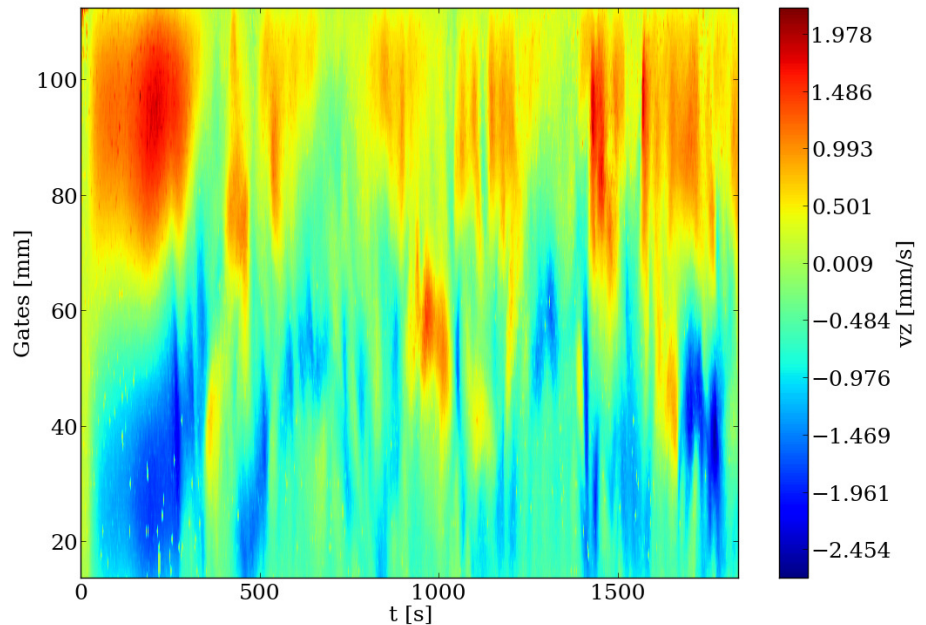

Figure 13: Flow pattern measured at the center of the container by $S = 10$. The scale for the flow pattern is used as a guide, only. Positive velocities, coloured in red, represent regions of downstream, while negative velocities, coloured in blue, represent region of upstream.
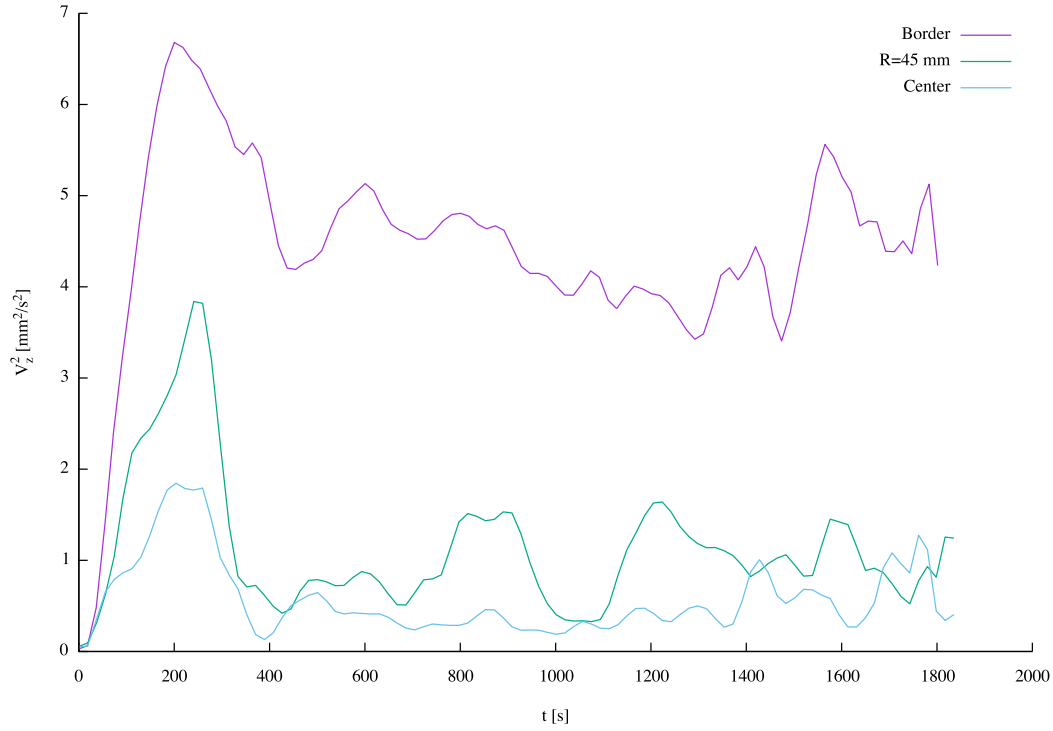
Figure 14: Plot of the kinetic energy for the three flow patterns. Bezier curves are used as a guide.

All these qualitative observations can be explained as a consequence of the skin effect and Navier-Stokes equations. In fact, being the $\nabla \times F$ confined to a thin layer, *i.e.* to the corners of the container, outside this forced region $\nabla \times F$ becomes almost negligible: the streamlines passing through the forced region must then circulate in a free-forced region where energy, momentum and vorticity are dissipated [64].

To show why the streamlines must not close in the unforced region Davidson et al. formulated the advection equation from the inviscid Navier-Stokes equation, since their analysis concerned a turbulent flow in an induction furnace [64]. Even though the present experiment deals with a flow which is apparent laminar, the kinematic viscosity ν of InGaSn is $3.4 \cdot 10^{-7}\frac{m^2}{s}$ so that the term of the Navier-Stokes equation concerning kinematic stresses becomes almost negligible. If a two dimensional flow is assumed, an assumption commonly accepted for induction furnaces, then the vorticity ω is $\omega = \frac{\partial u_y}{\partial x} - \frac{\partial u_x}{\partial y}$, while for any steady flow the total energy $H = \frac{p}{\rho} + \frac{1}{2}v^2$ must be considered. Therefore, the two dimensional flow is determined by the following equations regulating the vorticity:

$$\frac{D\,\omega}{Dt} = \mathbf{v}\nabla \cdot \omega = \frac{1}{\rho}(\nabla \times \mathbf{F})_z \tag{82}$$

and the energy H:

$$\frac{DH}{Dt} = \mathbf{v}\nabla \cdot H = \frac{1}{\rho}\mathbf{F} \cdot \mathbf{v} \tag{83}$$

It is clear that streamlines cannot close in the forced region; if that happened, energy H and vorticity ω would continuously increase, although it is possible to have streamlines closed in the unforced region (for example the constant vorticity flows studied by Batchelor [65]).

As noted in [64] there is a clear reason for the velocity decrease; on the other hand, the dissipation of energy, momentum and vorticity brings to a structure which is chaotic and unstable. Experimental and analytical studies have been proving those assertions in turbulent regime. Bojarevics et al. in a numerical simulation showed the presence of a radially propagating jet from the wall, which brings the turbulence inside the core of the fluid: flow structure turns out to be totally chaotic with a fast

evolution, in the order of seconds [67]. In addition, Umbrasko et al. [66] indicated how the velocity distribution, symmetrical in the first step, turns out to be completely asymmetrical, only the time averaged distribution being symmetrical.

It seems like there is a scarcity of works focused on laminar flow, since most authors focus on the turbulent regime. However, the idea according to which an asymmetry of flow structure is typical of a turbulent regime must be rejected: in fact, the measurements of the present work indicate how phenomena normally considered typical of turbulent flows are now documented for laminar flow regimes; interestingly, Gelfgat & Gorbunov , conducting their study in a similar situation, i.e. a vessel with a free surface, with small Reynolds number, around 500, noted fluid instabilities and a transition to what the authors called a turbulent regime [72]; their observations appear quite in agreement with the results proposed, even though it should be said that the term turbulence must be used with circumspection and great care.

4.1.2   *20>S>75*

The range between $S = 20 - 40$ is indicated by many authors, Fautrelle [11] and El-Kaddah & Skezely [24] to cite a few, the region where the maximum of velocities is expected. Nevertheless, in this section the range taken into account is extended to $S = 100$ because there is a strong analogy between the flow structures in this range, which differs remarkably from flow pattern for $S < 10$.

Figure 15, figure 16 and figure 17 show the flow pattern recorded for $S = 20$. The first notable observation concerns velocity, which is increased, as expected: however the increase is remarkable at the border of the container, while it is rather feeble outside this region, i.e. the energy is soon dissipated. Secondly, the flow structure presents some features which were unforeseen: for example, even though they are very feeble and hard to distinguish, during the spin up of the fluid, in figure 15, two secondary vortexes appear: from time to time the secondary eddies are suppressed and the primary vortexes expand. In regards to the other two plots, in the first phase these secondary vortexes are not detected and the so called typical double toroidal structure is found: however, as for $S = 10$, the fluid interested by secondary circulation is more chaotic and secondary vortexes appears when the motion is already developed, namely for $t \approx 950$ in figure 16 and $t \approx 750$ in figure 17.
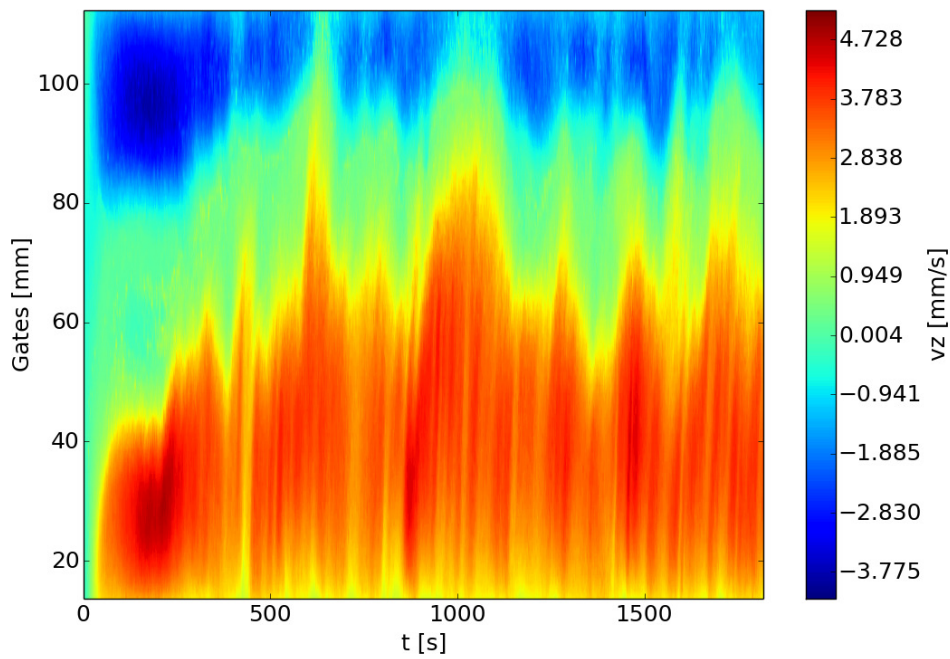
Figure 15: Flow pattern for $S = 20$ at the rim of the container. The scale for the flow pattern is used as a guide, only. Positive velocities, coloured in red, represent regions of downstream, while negative velocities, coloured in blue, represent region of upstream.
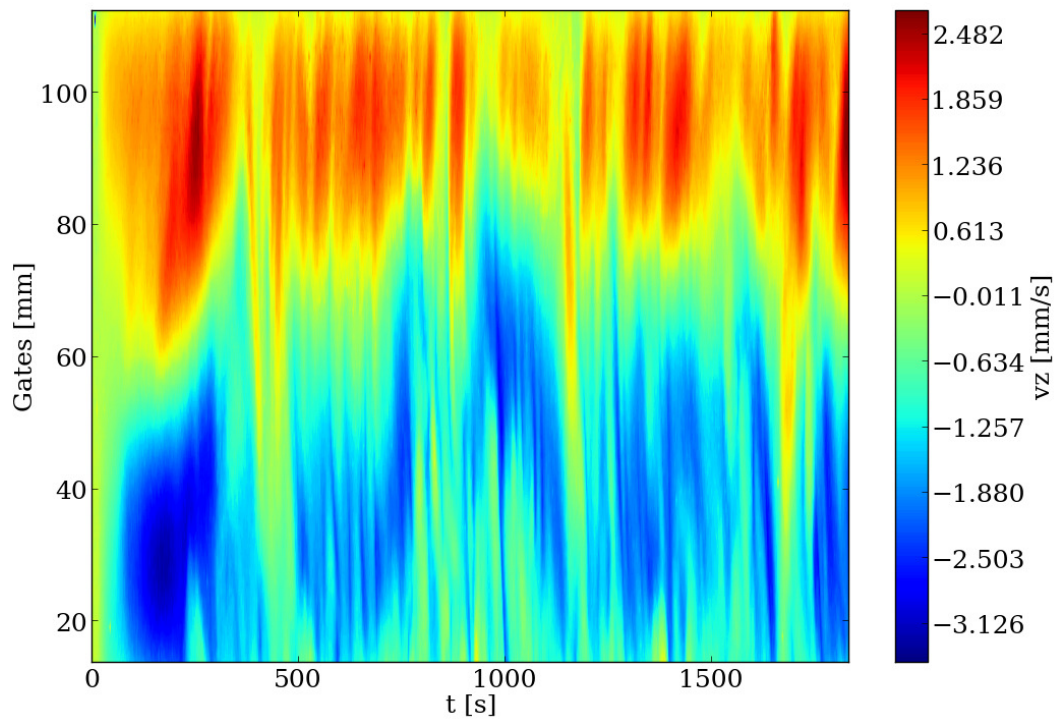

Figure 16: Flow pattern for $S = 20$ at the radial position $r/R = 0.5$. The scale for the flow pattern is used as a guide, only. Positive velocities, coloured in red, represent regions of downstream, while negative velocities, coloured in blue, represent region of upstream.
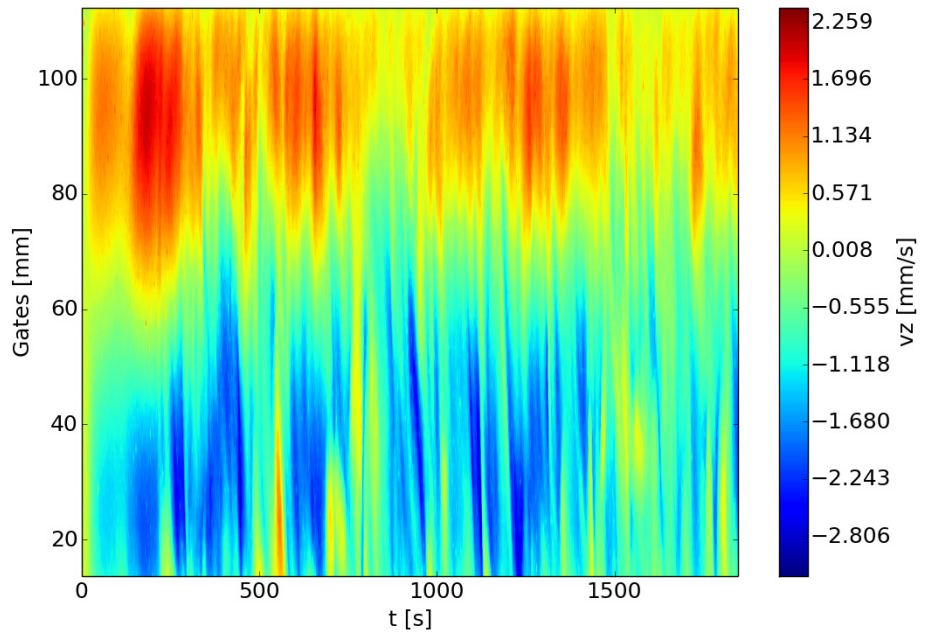
Figure 17: Flow pattern for $S = 20$ at the center of the container. A Bezier curve is used as a guide for the eye.

In figure 18 the kinetic energy is analyzed: as it can be clearly seen, the kinetic energy here is higher than for $S = 10$, as expected: the oscillations of energy are boosted, but there is any correspondence for oscillations among the measurements, proving that there are different regions of motion within the fluid. Again, we stress that the kinetic energy shows an increase only at the rim of the container.
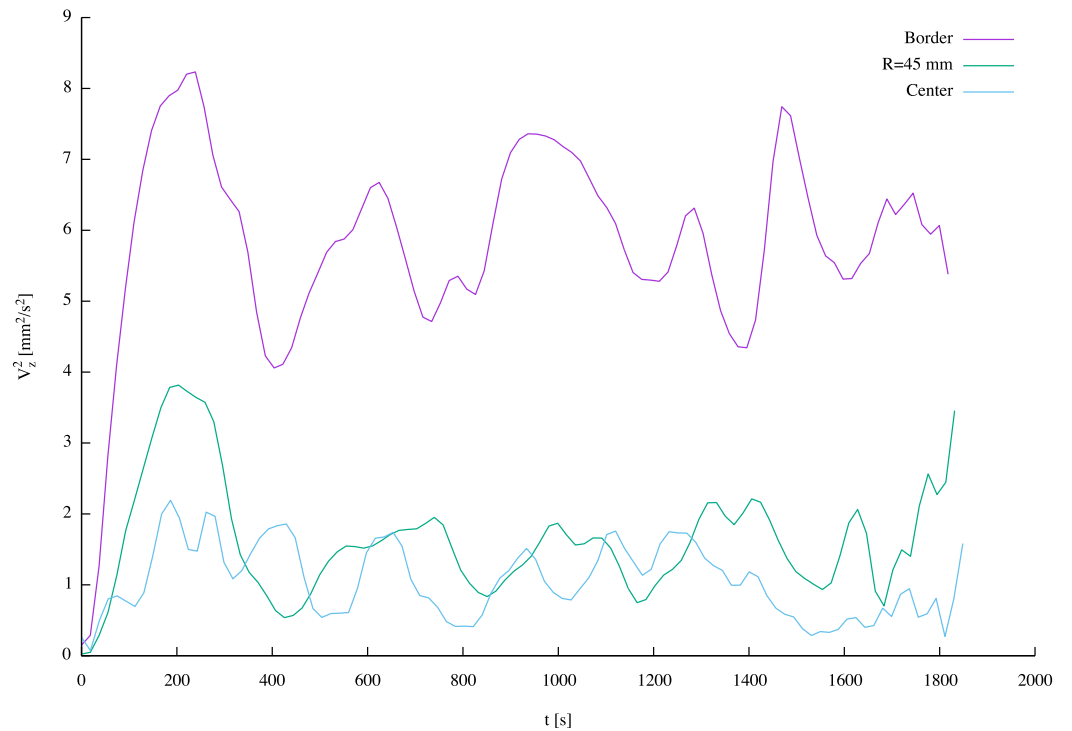

Figure 18: Plot of the kinetic energy for $S = 20$ for the three positions recorded. Bezier curves are used as a guide for the eye.
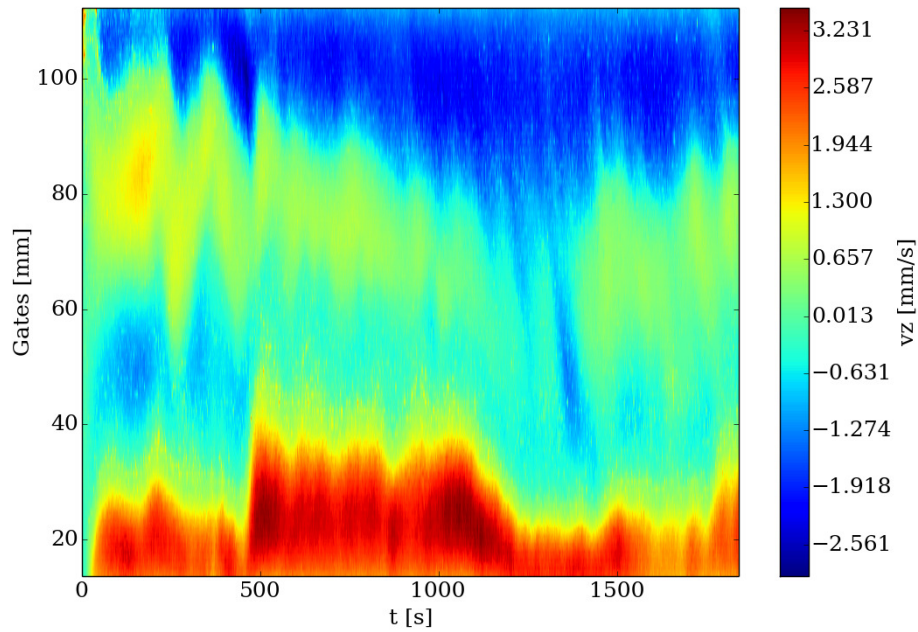
Figure 19: Flow pattern measured at the rim of the container for $S = 40$. The scale for the flow pattern is used as a guide, only. Positive velocities, coloured in red, represent regions of downstream, while negative velocities, coloured in blue, represent region of upstream.

A new series of plots present the measurements carried out for $S = 40$ in figure 19, figure 20 and figure 21 respectively. The first striking observation concerns the four eddies detected at the border of the container during the spin up, with the secondary eddies now stronger in comparison to the same position for $S = 20$. Four vortexes are detected also for the coordinate $\frac{r}{R} = 0.5$, although not exactly from the beginning, therefore the two secondary vortexes expand along the radial coordinate, before being again suppressed and reformed as already spotted for $S = 20$. The secondary vortexes are not found in the center of the container, even though by $t \approx 850s$ a small vortex appears in the region of upstream.
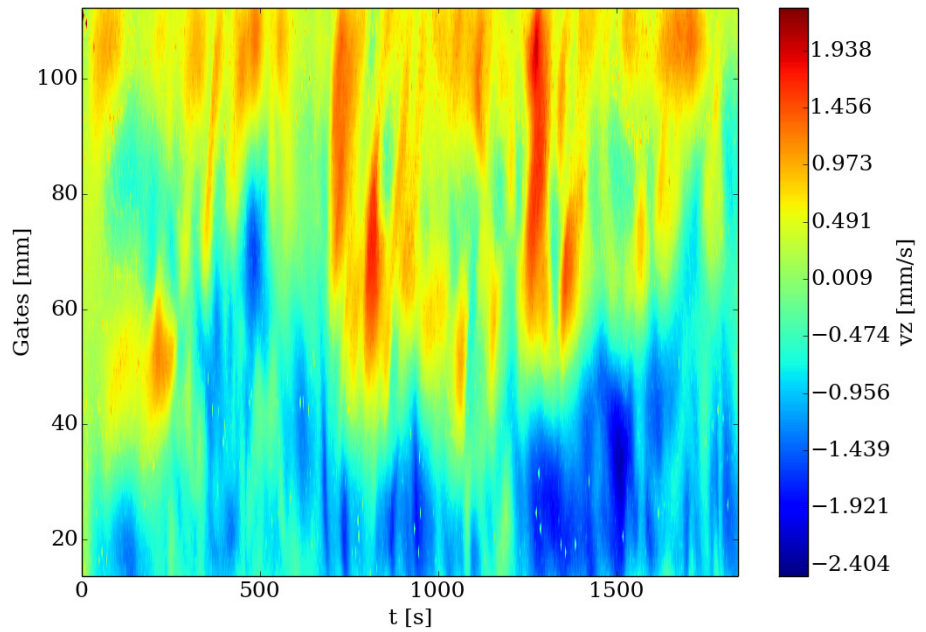
Figure 20: Flow pattern measured at the radial position $r/R = 0.5$ for $S = 40$. The scale for the flow pattern is used as a guide, only. Positive velocities, coloured in red, represent regions of downstream, while negative velocities, coloured in blue, represent region of upstream.
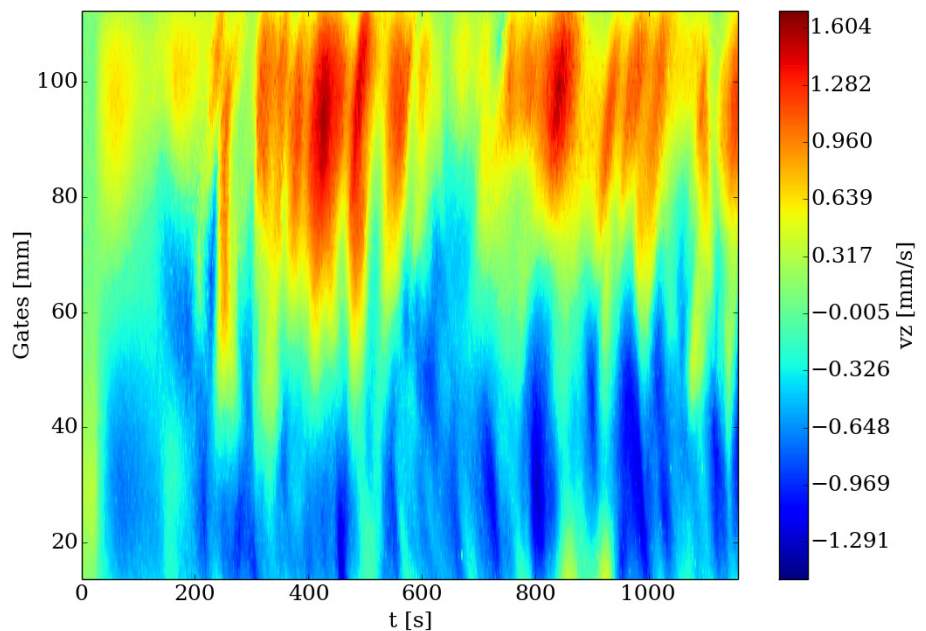

Figure 21: Flow pattern measured at the center of the container for $S = 40$. The scale for the flow pattern is used as a guide, only. Positive velocities, coloured in red, represent regions of downstream, while negative velocities, coloured in blue, represent region of upstream.

The kinetic energy for $S = 40$ is plotted in figure 22: in comparison with the plot for $S = 20$ the decrease of energy and oscillations is clear: the energy is less than half its previous value: interestingly in this case the maximum of the kinetic energy

is not recorded during the spin up. Moreover, there is not quantitative difference for the energy in the cases of secondary motion, i. e. for $\frac{r}{R} = 0.5$ and the center of the container; this means that the forced region is now strongly confined to the corners of the fluid and the energy is quickly dissipated.
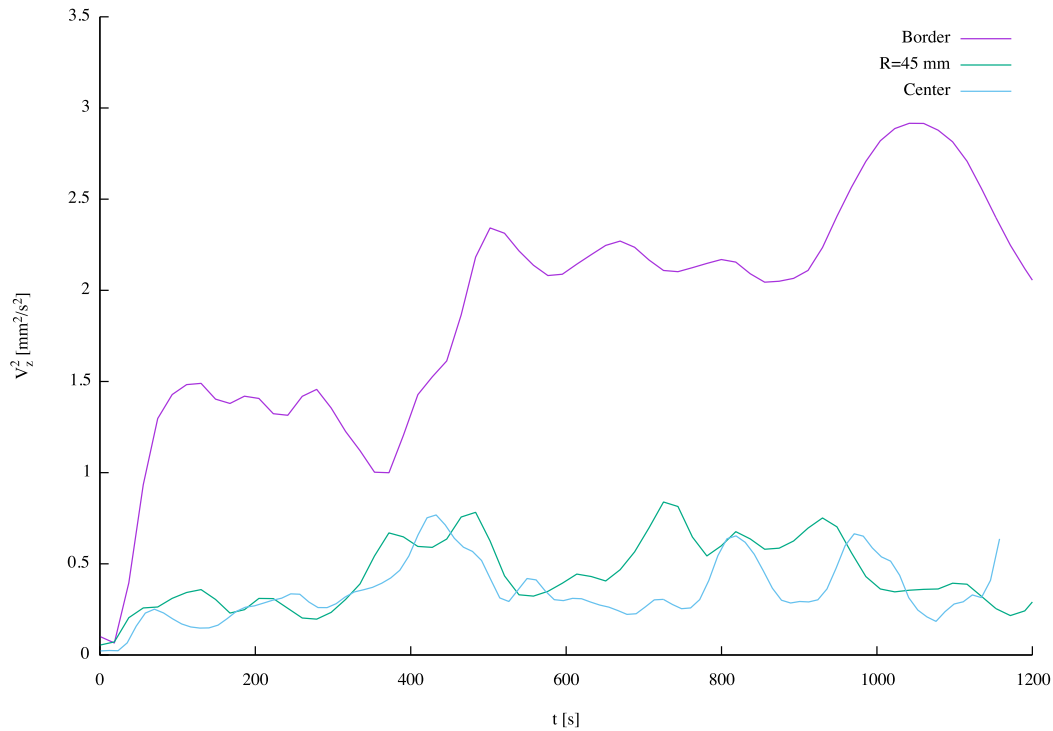

Figure 22: Plot of the kinetic energy for $S = 40$ for the three positions recorded. Bezier curves are used as a guide for the eye.

The results here presented offer a deal of interesting observations which, to the best of our knowledge, either have never been reported in literature or are not consistent with previous experiments. First of all, the observation concerning the four toroids recorded during the spin-up has no confirmation; the comparison with the initial pattern for $S = 10$, the so-called typical double toroidal structure, suggests that perhaps this structure is not so typical as one would expect: the presence of two vortexes seems a condition necessary, but not sufficient to describe the fluid flow. A structure composed by two eddies would be consistent with the distribution of Lorentz forces, but does not explain how two other secondary vortexes appear. Secondly, as it has been already pointed out for $S = 10$, being the fluid flow laminar, one would not expect oscillations so remarkable of kinetic energy for $S = 20$ and such a strong decrease for $S = 40$. Thirdly the kinetic energy for $S = 40$ indicates that the maximum of energy is not recorded during the spin up: due to reasons of space, it is not possible to show that such a behaviour was observed also for $S = 50$; these cases are not consistent with what has been observed for all the other cases. Unfortunately, it is not totally clear the reason of this discrepancy; it is probably due to the distribution of Lorentz forces within the fluid.

The presence of more than two toroids was at first noticed by Bednarz [15]: he showed how the primary vortexes, interacting with the wall of the furnace, generate shear forces which are responsible of the secondary vortexes. He noticed also how those secondary vortexes can be temporarily suppressed by the primary vortexes: however, his model describing the development of eddies seems in contrast with the measurements already shown. Furthermore, it is not clear whether Bednarz 's observations would be valid for different shielding parameters, say $S = 20$ and $S = 30$. In the experiment conducted by Taberlet & Fautrelle, the measured flow pattern for $S = 30$ consisted of two eddies [20]. Their measurements were later compared with a numerical simulation in the work of El-Kaddah & Skezely [24], who confirmed for $S = 30$ a double toroidal structure. It is not easy to indicate the

reasons why there are such discrepancies with the studies quoted: a reason could be attributed to the difficulties, stated by Taberlet & Fautrelle, to measure the evolution of fluid flow, a difficulty overcome in the present experiment thanks to DOP 2000, whose spatiotemporal information is one of the main advantages with respect to other tools [53]: another reason could be attributed to a not sufficient sensitivity of the instruments used by Taberlet & Fautrelle and El-Kaddah & Skezely , namely the directional probe and the hot film anemometer.

4.1.3   *S>100*

According to predictions, the last series of measurements, should have shown a decrease of motion within the fluid: however, these predictions have been proved wrong. In fact, as it can be seen in figure 23, the mean velocity is diminished in comparison to $S = 20$ but increased in comparison to $S = 40$; therefore $S = 100$ appears as a local maximum. As far as the flow structure is concerned, a strong modification from the pattern in the two previous sections is quite clear: the position of the two secondary eddies is shifted to the bottom and the top of the container; again, as it has already been observed, the secondary vortexes can be temporarily suppressed. In regards to main eddies, they show oscillations in order of tens of seconds, but their size remains almost constant throughout the recording time.
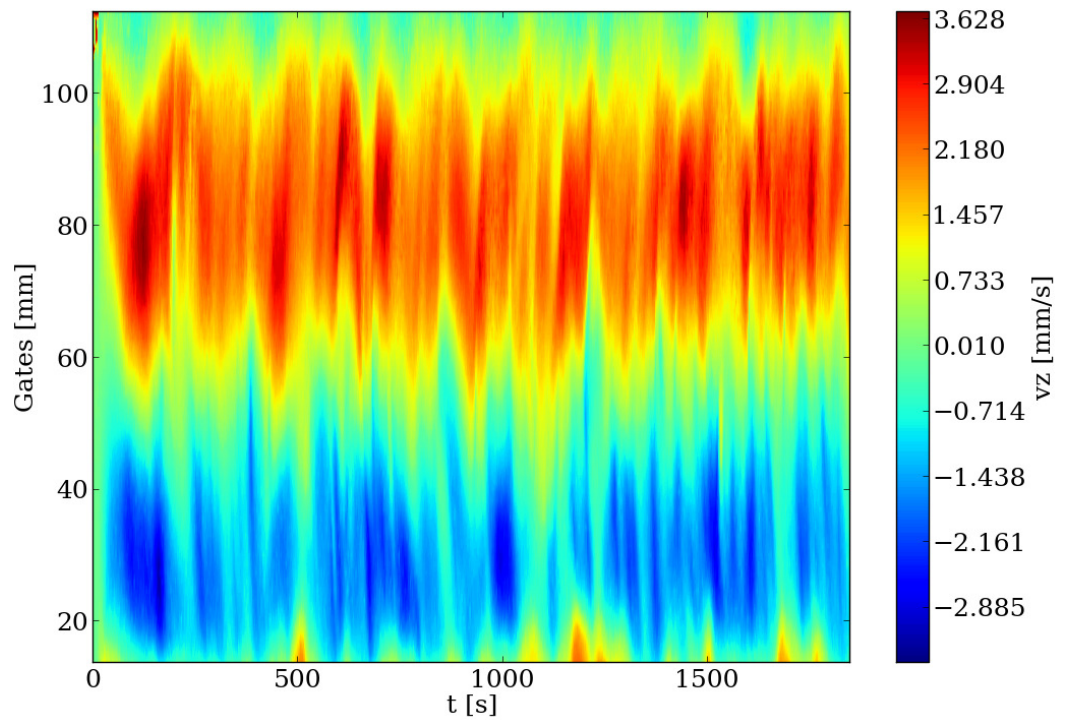

Figure 23: Flow pattern measured at the rim of the container for $S = 100$. The scale for the flow pattern is used as a guide, only. Positive velocities, coloured in red, represent regions of downstream, while negative velocities, coloured in blue, represent region of upstream.

   The subsequent measurement reported in figure 24 shows how the flow structure is radically changed: first of all, during the spin-up phase the four-vortexes structure is no longer evident, in its stead we observe a rather feeble secondary vortex appearing at the top of the container. However, even though it is hard to detect, another secondary vortex appear between $t \approx 300s$ and $t \approx 1200s$. Secondly the ratio of size between the main vortexes is now strongly modified, with the vortex represented in red (region of downstream) now reduced; moreover, the oscillations of the main vortexes are now increased. Finally, the mean velocity is decreased in comparison to $S = 100$.
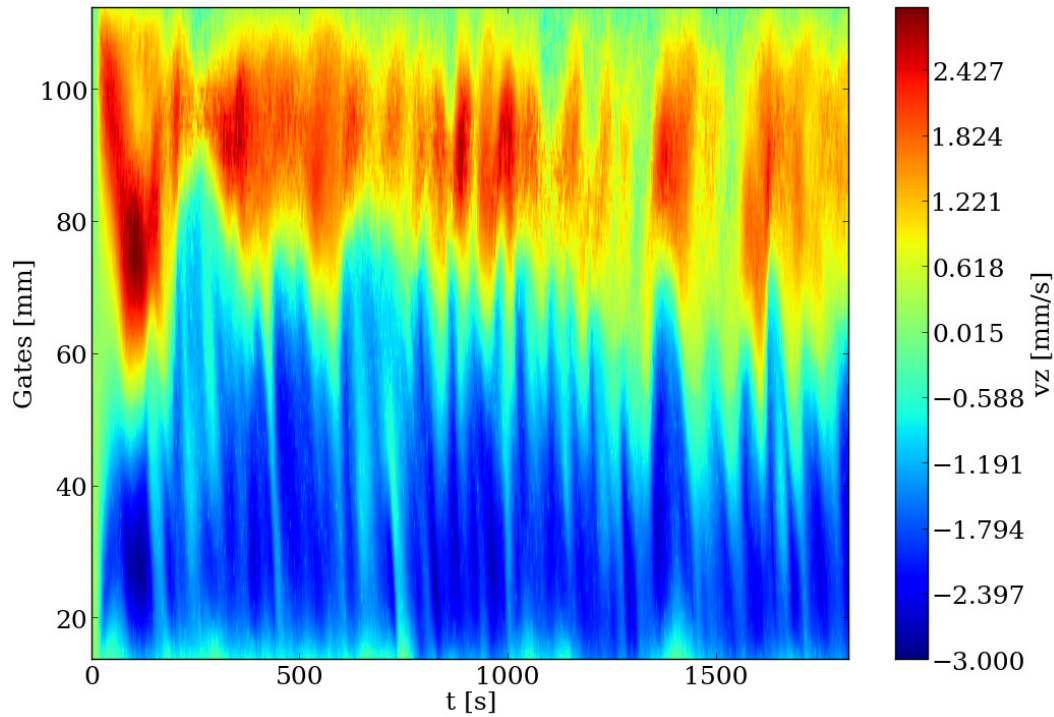
Figure 24: Flow pattern measured at the rim of the container for $S = 150$. The scale for the flow pattern is used as a guide, only. Positive velocities, coloured in red, represent regions of downstream, while negative velocities, coloured in blue, represent region of upstream.

The evolution of the flow pattern is now completed if one observes figure 25, where we plot the flow pattern as recorded at the rim of the container for $S = 200$. The first striking observation is that we do not observe the evidence of a double toroidal structure anymore, since one of the so called main eddies disappears: thus for some periods of time the fluid is characterized by a region of upstream, except for a very small secondary vortex detected at the top of the container. Thus one would be led to consider that there is only one leading vortex and probably the vortex represented in red (downstream) should be downgraded to a secondary vortex. Note how the velocity is not diminished in comparison to $S = 150$: this suggest that probably the force distribution is for both cases strongly confined to the borders and all the fluid is affected by a secondary motion.

Such an interesting flow pattern as shown in figure 25 needs to be better understood. Therefore in figure 26 and figure 27 one can see the global behaviour of the fluid. As far as the radial position $\frac{r}{R} = 0.5$ is concerned, the structure composed of one main leading vortex is here confirmed, even though, as it can be seen by $t \approx 600$, the region of downstream changes sign and becomes a region of upstream; such an inversion of the main vortex has never been detected before. In regards to the secondary vortex already present at the top of the container already present in figure 25 it is clearly stronger; therefore the eye of this vortex is to be found not near the rim of the container, but shifted.
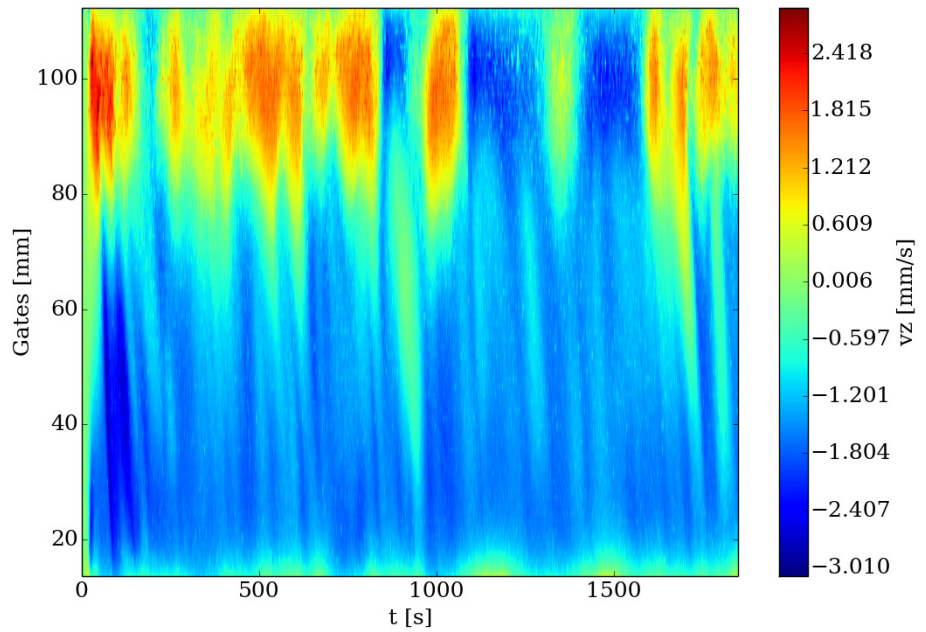
47

Figure 25: Flow pattern measured at the rim of the container for $S = 200$. The scale for the flow pattern is used as a guide, only. Positive velocities, coloured in red, represent regions of downstream, while negative velocities, coloured in blue, represent region of upstream.
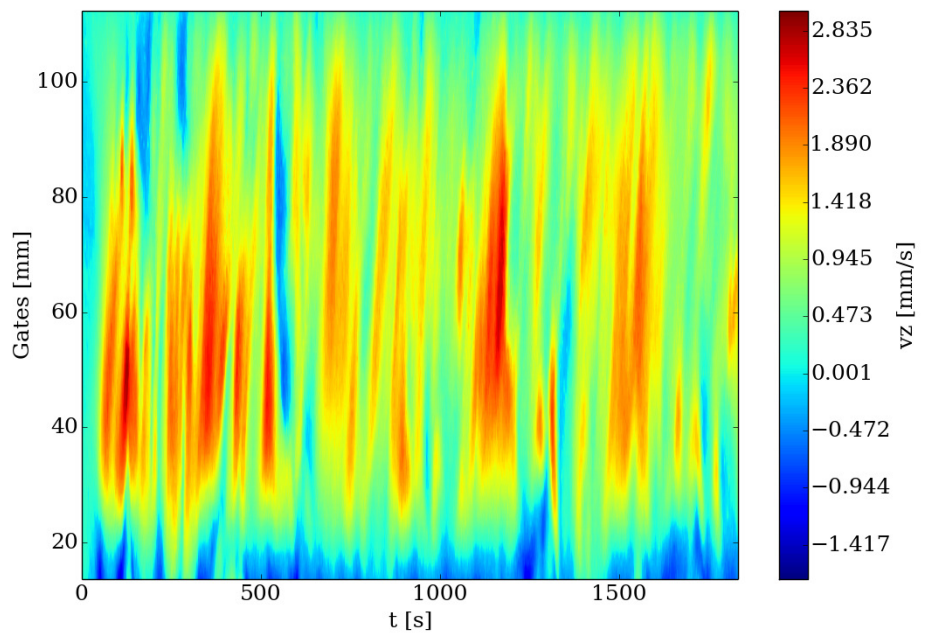
Figure 26: Flow pattern measured at the radial position $r/R = 0.5$ for $S = 200$. The scale for the flow pattern is used as a guide, only. Positive velocities, coloured in red, represent regions of downstream, while negative velocities, coloured in blue, represent region of upstream.

Figure 27 represents the temporal evolution of the flow pattern at the center of the container: firstly, it should be noted that the toroids are spotted after a delay not visible in other measurements. The confinement of forces to a very thin layer leads to

48

a decrease of motion within the fluid , as a consequence it takes more time for eddies to be formed. Secondly, as already observed, the pattern is formed by three toroids, with a principal toroid and two secondary toroids: unlike the previous measurements for $S = 200$, the structure is stable and there is no change of sign for the leading vortex as it has been observed in figure 26 or oscillations so remarkable as in figure 25. Note that a very weak third toroidal vortex appears for $t \approx 650$ at the bottom of the container.

Figure 27: Flow pattern measured at the center of the container for $S = 200$. The scale for the flow pattern is used as a guide, only. Positive velocities, coloured in red, represent regions of downstream, while negative velocities, coloured in blue, represent region of upstream.
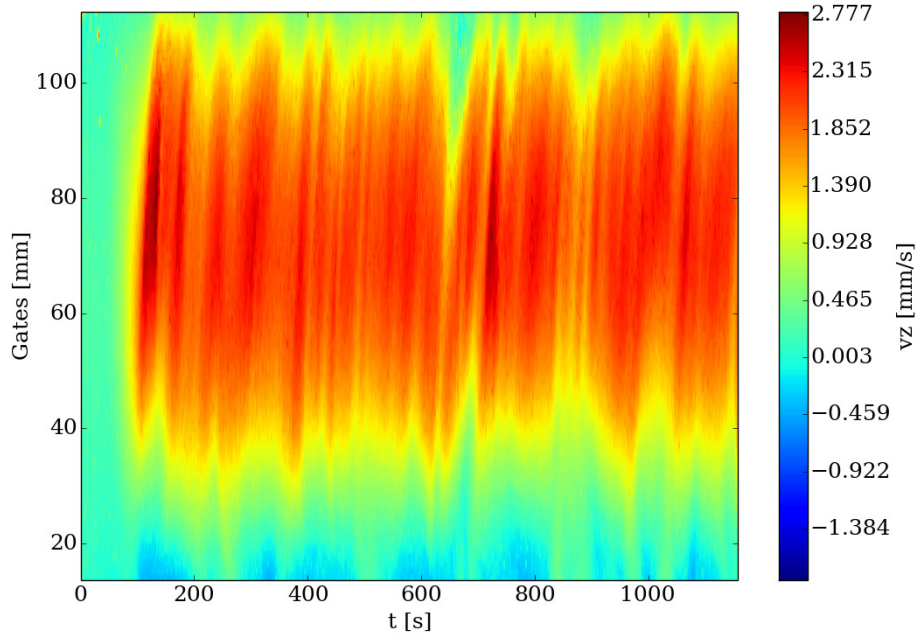
As previously done we analyze the trend of the kinetic energy: in figure 28 we show the comparison of the three different shielding parameter described in this section. The maximum of energy is again recorded during the spin-up, even though the area subtended is now strongly reduced, i.e. there is a fast decrease after the spin up. The presence of strong oscillations for all the three cases, as it was already suggested by the flow patterns, is here confirmed. Notably, except during the spin up, we do not observe a big difference in kinetic energy between the three measurements, the decrease for $S = 200$ being not so sharp as one would expect.

Finally we analyze the kinetic energy to compare the measurements of $S = 200$. The most interesting observation concerns the difference of motions within the fluid, which are now reversed, as the kinetic energy recorded at the center of the container is always higher than the position $R = 45$ mm and higher than the kinetic energy at the rim of the container, except for the spin-up. It is not clear the reason behind this reversal of the motion within the fluid; probably the inertial forces keep the motion at the core of the fluid while the forces are now easily dissipated at the border of the container.
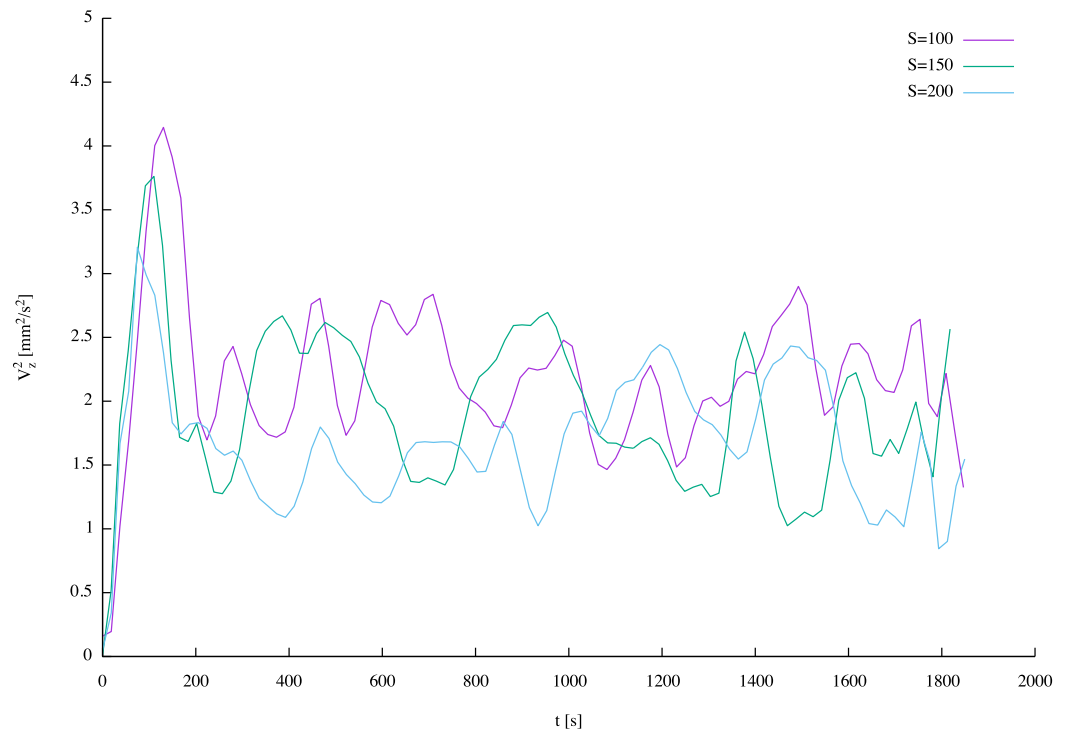
Figure 28: Trend of kinetic energy recorded at the rim of the container for $S = 100$, $S = 150$ and $S = 200$. Bezier curves are used as guide for the eye only.
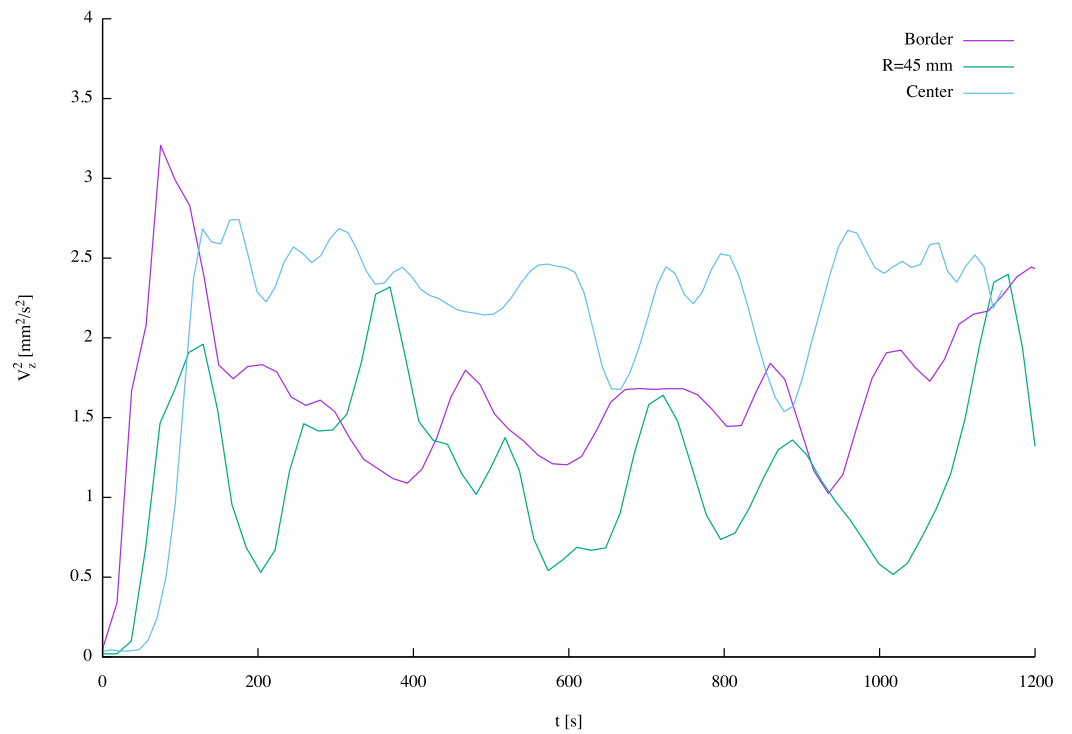
Figure 29: Trend of kinetic energy of for $S = 200$. Bezier curves are used as a guide for the eye only.

As far as previous studies are concerned, unlike the range $S \in [20, 75]$, there is a consistency with the results just presented. The experimental study of Taberlet & Fautrelle shows, for $S = 166$, a structure composed of three vortexes, with a secondary vortex extending less than a quarter of the radius pool [20]. Unfortunately the authors were not able to provide a temporal evolution of the flow structure, due

to the difficulties already quoted in the previous comparison with $S = 30$. The only difference with the flow pattern of Taberlet & Fautrelle consists in the very feeble vortex detected in the present experiment at the bottom of the container; probably the tools available to the authors, used in a turbulent regime, did not allow to discover this rather small vortex.

The subsequent work by El-Kaddah & Skezely , carried out with the same technique, shows a result which appears more consistent with the present research: as a matter of fact for $S = 166$ four vortexes were measured [24]. Comparing their measurements with the numerical simulation, as already reported in the introduction, the authors were doubtful about the discrepancy between simulation and measurements and they could not state for sure which one could be misleading. However, the comparison with the flow pattern of figure 24 and the flow pattern of Taberlet & Fautrelle would suggest that the discrepancy should be attributed to the computational model.

4.2   MAXIMUM OF KINETIC ENERGY

The existence of a frequency range where the maxima velocities can be found has been pointed out by many authors (a review concerning this point is to be found in Section 1). Most of the authors seem to agree to a maximum for mean velocities for $S \approx 40$, while according to Bednarz the maximum is in the range $15 < S < 20$. The existence of this range is straightforwardly of practical interest as far as it concerns the project Sikelor ; it has been already pointed out the necessity of a compromise between a too high velocity, which would drag the impurities away from the melt, and a too low velocity, which would not allow to confine the impurities to the border of the container.

Being one not interested only in the flow speed of the fluid, but in the overall behaviour of the fluid, it is more interesting to plot the trend of kinetic energy. The maximum of kinetic energy for all the measurements as a function of S is plotted in figure 30. First of all, one notes that until $S = 75$ the three curves show the same trend, with the expected difference of motion within the fluid. However, after that, while the curve representing the border of the container and the radial position $R = 45$ mm show a partial increase followed by a decrease, the curve representing the center of the container show a very strong increase: such a behaviour was not expected.

In regards to previous works, Bednarz stated that the maximum of flow speed should be around $S = 16$ [15], in agreement with the theoretical predictions of Damaskos [13] and MacAnlis [14]. The results of Bednarz are reproduced in 31. Even though the maximum in figure 30 is not exactly in this position, there is a clear consistency with the work of Bednarz . Note that Tir similarly found the maximum of kinetic energy in a coreless induction furnace for $S = 20$ [70]. On the other hand, there is no agreement with the results of Trakas et al. who stated that near the wall the velocity should reach a saturation value for $S = 18$ [19], although the author stressed that there was any evidence of such a saturation for higher S. Taberlet & Fautrelle detected a maximum of mean velocity for $S = 40$ [20]; the discrepancy is probably attributable to the lack of measurements of the authors in the range $S = 10 - 20$.
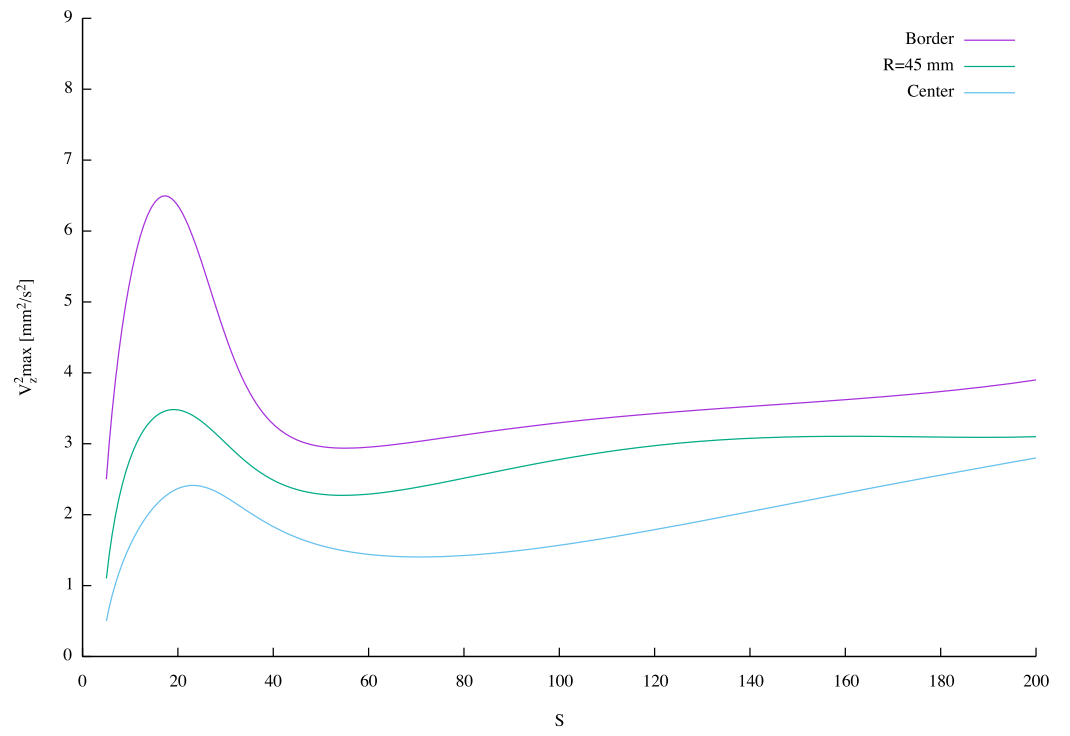
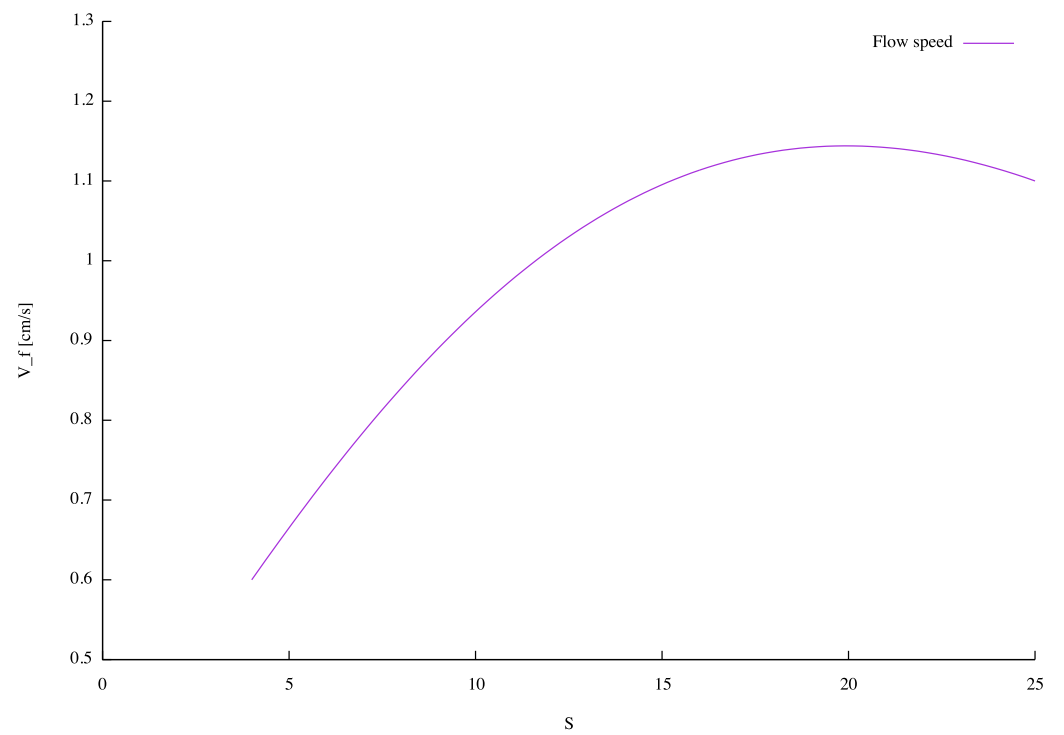Figure 30: Trend of maxima values of kinetic energy.

Figure 31: Flow speed versus S, according to the Phd thesis of Bednarz .

5

COMPARISON WITH A NUMERICAL SIMULATION

While the first stage of the experiment was being completed, i.e the measurements concerning the not symmetrical system, the results already appeared not totally in agreement with previous studies. Therefore a three-dimensional simulation conducted with OPENFOAM [1] was carried out firstly in order to present a comparison with the experimental results, secondly to indicate which shielding parameters and which sensor positions could be useful. The simulation was performed in three dimensions because such instabilities of flow patterns would have been reasonably bad understood with a two dimensional measurements, i.e. in two dimensions too simplifications would occur.

In this section it is given as an example the simulation for $S = 10$, not symmetrical system. The flow pattern is presented in figure 32 and it is readily seen how there is any qualitative difference between the symmetrical and the not symmetrical system.

First of all, it is proposed in figure 33 the temporal evolution of the flow pattern: after a first stage in which is detectable a symmetrical structure, in another temporal stage this structure radically changes and a double toroidal structure as it has always been described is not present any more. The structure becomes rather chaotic and it is hard to predict its evolution: the eddies oscillate, shrink and grow, and even decay and new ones develop. Three vortices can be recognized, the largest one on top, in the right half of the computational domain. Note the low velocity scale at which the extremely slow large-scale fluctuations occur. This observation confirms the idea that the double toroidal structure is present only during the spin up of the fluid: in turbulent regime this was already shown by the numerical simulations of Bojarevics et al. [67] and Umbrasko et al. [66]. The 'disappearing' of symmetry can be visualized in terms of vorticity in figure 34: thus one understands how because of instabilities flow structure changes dramatically.

---

1 The simulation was implemented by Dr. Vladimir Galindo
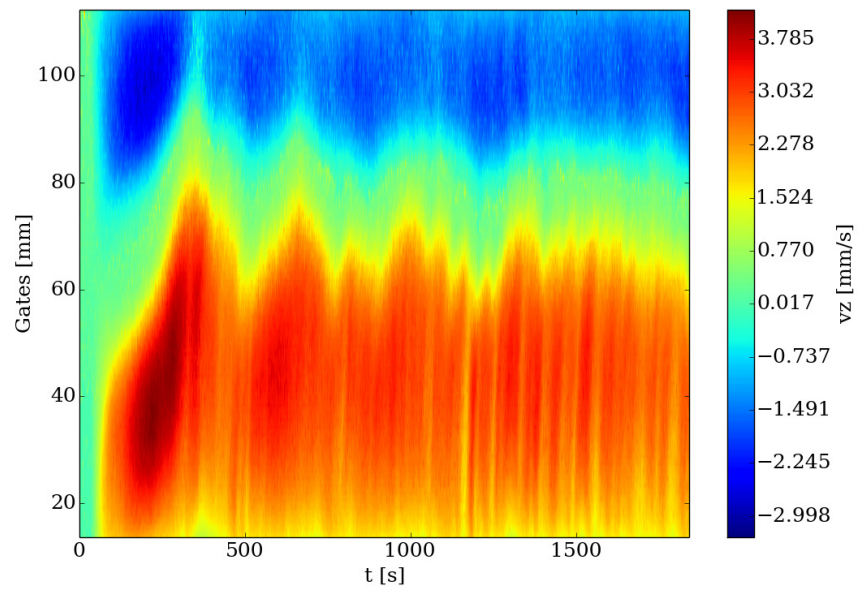
Figure 32: Flow pattern measured at the rim of the container for $S = 10$, system not symmetrical. The scale for the flow pattern is used as a guide, only. Positive velocities, coloured in red, represent regions of downstream, while negative velocities, coloured in blue, represent region of upstream.
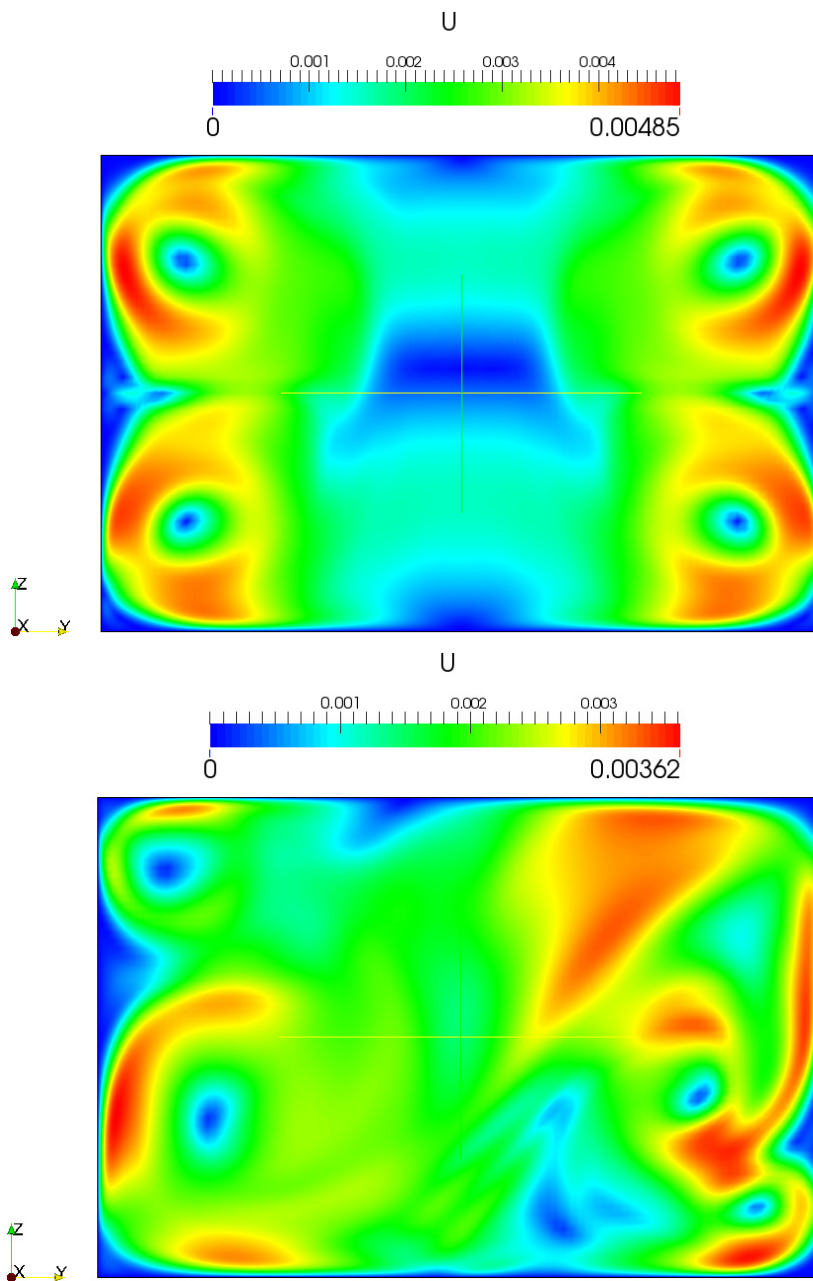
Figure 33: Plots of the absolute value of the mean velocity in a vertical section through the centre of the fluid volume at two instants of time. The left panel for $t = 500$ s shows an almost perfectly symmetric double-toroidal flow as it develops in the early stage after the spin-up. In the right panel a deformed double-torus with the upper one significantly smaller than the lower one can be seen to the left.

Figure 34: Fluid vorticity visualized *via* criterion Λ_2, Jeong et Hussain [78]. After a first stage the symmetry is broken and the structure is strictly irregular.

Figure 35: Evolution of meridional kinetic energy and of azimuthal kinetic energy. The rise of the azimuthal kinetic energy shows how the motion within the fluid is completely three-dimensional.

Figure 35 shows an interesting result: the structure changes at $t \approx 1100$, with the ϕ component of the flow raising while the meridional flow faces a decrease; moreover it is clear how oscillations of kineti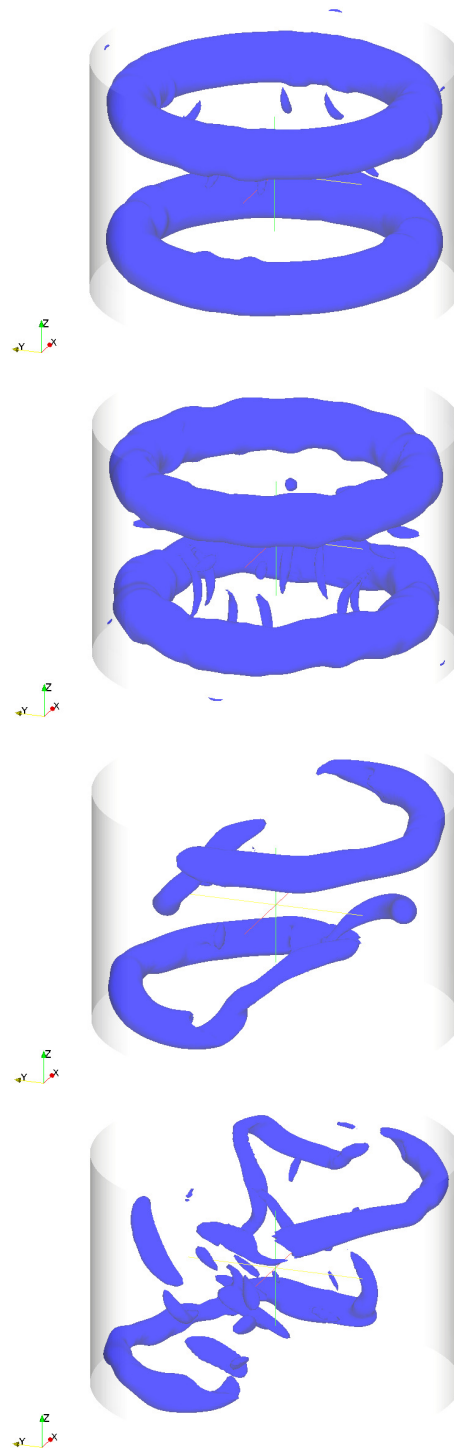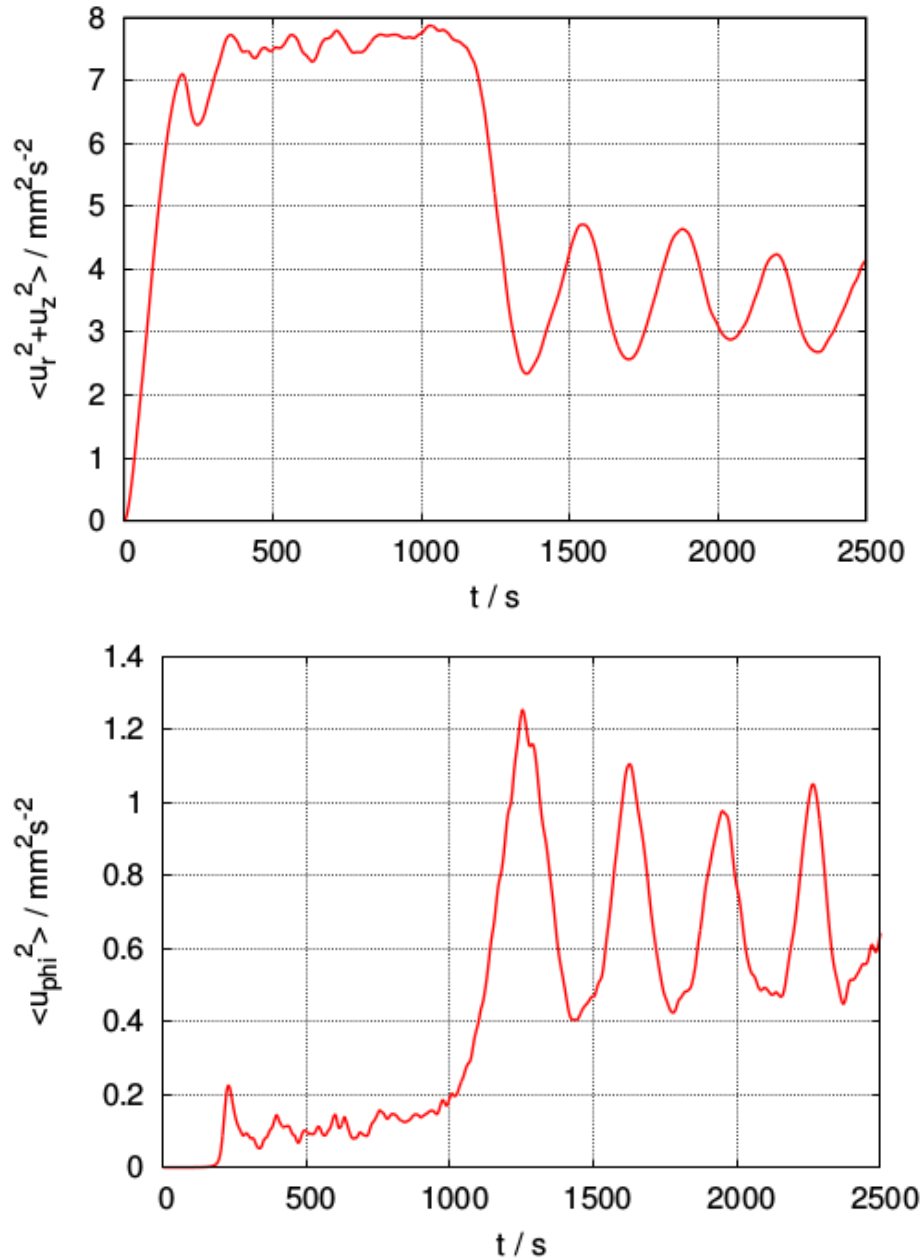c energy are found for the numerical simulation as well. Thanks to the simulation one can reasonably explain the cause of eddies oscillations, which are due to a three dimensional movement of vortexes: apparently just one sensor in a fixed position does not allow to detect where the maximum of velocity is to be found, because of continuous change of position of vortexes.

The discrepancy with the evolution of kinetic energy shown in the measurements is due to the different method of calculation: the kinetic energy plotted from the measurements is the average kinetic energy just of the $\langle v_z \rangle$ component, whereas the simulation presents the kinetic energy integrated over the whole volume. Therefore the numerical simulation and the measurements lead to infer that, even if the regime is laminar, the fluid shows a not stationary behaviour with a clear three dimensional movement of vortexes. The flow is not more just meridional, but the ϕ component must be taken into account as well.

6

CONCLUSION AND RECOMMENDATIONS FOR FUTURE WORKS

As mentioned above, the dependence of flow structure on frequency has been already stated by several authors [19, 20]. Secondly, authors like Gelfgat & Gorbunov observed oscillations of velocities in the case of laminar flow [72]. Thirdly, the idea of a three dimensional motion of the fluid has been already suggested [73]-[76].

As far as the dependence of flow structure on frequency is concerned, according to the measurements the difference is greater than expected. Three different flow patterns have been identified for different S. The firs flow pattern is the double toroidal structure is the double toroidal structure, confirmed until $S = 10$. For $S > 20$ a structure composed by four vortexes appears as the typical flow structure: finally for $S > 100$ there is a dramatical transformation of structure into a pattern composed by only one leading vortex and two secondary vortexes. To the best of our knowledge, such a distinct difference has never been observed before. Another interesting result concerns the oscillations of flow structure observed for all the measurements, except $S = 5$: those oscillations, spanning in order of tens of seconds, seem scarcely reported in literature in regards to laminar flow.

Gelfgat & Gorbunov pointed out that the cause of instabilities is attributable to shear flows [72]: however, it is not fully understood why there is such a great difference of structure as S changes. First of all, it should be noted that probably the distribution of Lorentz forces has not been totally studied; as a matter of fact, just the variation of distribution of Lorentz forces could cause such a difference of flow pattern. Secondly, the measurements proposed lead to consider that the problem of determine which is the characteristic fluid velocity is not so straightforward as it would seem: measuring only $\langle v_z \rangle$ or $\langle v_r \rangle$ is not sufficient to understand the evolution of motion within the fluid. Thirdly the comparison with the simulation shows how the nature of motion of fluid is fully three-dimensional.

A deeper investigation should be carried out, both experimental and numerical: the three dimensional nature of the fluid asks a more precise study, especially from the experimental point of view; it would be interesting to carry out measurements of more velocity components simultaneously, $\langle v_z \rangle$ and $\langle v_r \rangle$ for example. Considering the fact that the vortexes tend to move, even to rotate if one takes into account $\langle v_\phi \rangle$ component, such a movement is obviously badly mapped only measuring one component; thus a new system is needed. Thus one would have elements to comprehend and maybe to predict the evolution of flow structure.

New researches should focus on the increase of frequency, for two reasons: first of all, it would be interesting to understand if there are any variations of flow structure as S increases, even though a measurement performed for $S = 1044$ suggests not a great difference with the for $S > 100$. Secondly, the increase of frequency appears important for the application of the project Sikelor : as a matter of fact, the velocities recorded for $S = 200$ are too high and the application of LKF forces would be not efficient for such velocities.

7

ACKNOWLEDGEMENTS

8

Ormai da molto tempo la produzione di silicio per la costruzione di pannelli solari é aumentata enormemente, grazie agli investimenti nel settore dell'energia rinnovabile: nonostante tale settore proceda a pieno ritmo, permangono molte criticitá produttive. In particolare circa la metá del silicio viene perduto durante il processo di creazione dei wafers di silicio. Da ció ne consegue che l'esigenza di ideare soluzioni tecnologiche che permettano il riutilizzo di questa enorme quantitá di silicio risulta fondamentale per l'abbattimento dei costi di produzione e di smaltimento.

Il progetto europeo Sikelor [30], nato dalla collaborazione fra alcune universitá ed aziende appartenenti a paesi membri dell'unione europea, ha come obiettivo quello di elaborare metodologie industriali che permettano di purificare il materiale di scarto proveniente dall'industria del silicio, ad un prezzo che possa essere competitivo con il silicio vergine.

ll dipartimento di Magnetoidrodinamica del centro di ricerca HZDR collabora al progetto Sikelor svolgendo ricerche sull'applicazione delle forze di Leenov-Kolin (LKF) [31]. Tali forze di separazione elettromagnetica, se utilizzate in un forno ad induzione, come quello proposto da Dughiero et al. [28], permetterebbero di confinare le impuritá presenti nel metallo fuso in prossimitá delle pareti del forno. Da qui potrebbero poi essere rimosse in seguito ad un processo di solidificazione.

L'applicazione delle forze di Leenov-Kolin, nonostante il successo documentato in alcuni esperimenti [34, 35], risulta ancora discussa in maniera controversa in letteratura, dato che un movimento eccessivo del metallo fuso impedirebbe l'accumulo delle impuritá nelle pareti, mentre d'altro canto é necessario che il fluido si muova affinché le impuritá possano essere rimosse. Risulta quindi di fondamentale importanza individuare entro quali limiti esse siano applicabili.

L'espressione delle forze di Leenov-Kolin ricavata da Makarov et al. [33], mostra come queste forze dipendono dalla frequenza del campo di induzione magnetica applicato: é noto che, per un qualsiasi metallo allo stato liquido, l'interazione tra il campo magnetico e le correnti indotte all'interno del metallo (forza di Lorentz) creano dei moti convettivi, i quali strutturano il fluido secondo un modello denominato struttura a due vortici, in inglese 'Double toroidal structure'.

La presenza di questa struttura sembra confermata da molti studi, numerici e sperimentali; tuttavia, come sottolineato in [39] e [40], non tutte le caratteristiche di questa struttura sono state chiarite, in particolare la sua variazione in funzione della frequenza. Infatti secondo alcune ricerche, come dimostrato da Bednarz [15], esistono delle discrepanze tra il modello teorico e i risultati sperimentali: la comparsa di vortici secondari in alcune finestre temporali da un lato e la comparsa di instabilitá nella struttura del fluido dall'altro dimostra come siano necessarie nuove ricerche.

Dal momento che le forze di Leenov Kolin vengono applicate tramite un campo magnetico alternato, noto nella letteratura anglosassone con l'acronimo AMF, é necessario indagare con piú precisione come l'interazione delle forze di Lorentz con le correnti indotte modifichi la struttura dei moti convettivi.

L'esperimento qui descritto si é prefisso lo scopo di indagare la variazione della struttura del fluido in funzione della frequenza di un campo magnetico applicato. Un sistema costituito da due bobine é stato posto attorno ad un contenitore con all'interno una lega eutettica (InGaSn): una fonte di alimentazione connessa ad un generatore di frequenza e ad un amplificatore di corrente produceva una corrente, la quale, circolando nelle bobine, permetteva di creare il campo magnetico richiesto. Grazie al sensore ad ultrasuoni DOP 2000, é stato possibile effettuare misurazioni di

velocitá (della sola componente $\langle v_z \rangle$) all'interno del fluido che hanno permesso la ricostruzione dei suddetti moti convettivi.

E' ormai prassi che gli esperimenti siano condotti seguendo dei numeri adimensionali, che permettono un facile confronto tra esperimenti: pertanto, al posto della frequenza, si é preferito utilizzare il parametro adimensionale S, noto nella letteratura come 'Shielding Parameter', che tiene conto non solo della frequenza ma anche della geometria del sistema.

Date alcune limitazioni degli strumenti a disposizioni, non é stato possibile effettuare misure per frequenze al di sotto della soglia della frequenza di 25 Hz, che corrispondeva ad $S = 5$, né al di sopra di 960 Hz, $S = 200$. Inoltre alcune limitazioni riguardanti l'amplificatore non hanno permesso di raggiungere velocitá all'interno del fluido che superassero la condizione di regime laminare.

Le misurazioni di velocitá sono state effettuate spostando il sensore in tre diverse posizioni all'interno del fluido, cioé al bordo del contenitore, al centro e a metá fra il contenitore e il centro. Questa decisione é stata presa considerando che rilevazioni in una sola posizione non avrebbero permesso di rilevare con precisione la struttura del fluido.

In una prima fase dell'esperimento, le bobine si trovavano in posizione non simmetrica rispetto al contenitore del fluido: dopo i primi inattesi risultati, che indicavano la presenza di oscillazioni nella struttura del fluido, si é deciso di riportare le bobine in posizione simmetrica rispetto al container, principalmente per due ragioni: innanzitutto, perché la maggior parte degli esperimenti sono stati effettuati con una sistema a geometria assial-simmetrico, e in secondo luogo, essendo non esattamente chiara la causa delle instabilitñella struttura del fluido, é parso necessario semplificare la geometria del problema.

I risultati che sono stati ottenuti dimostrano alcuni fenomeni che, a quanto risulta dalle nostre conoscenze, non sono stati mai riportati in letteratura: in primo luogo, oscillazioni della struttura del fluido, anche estremamente marcate, sono state rilevate per tutte le misure, escluso il caso riguardante $S = 5$. Queste oscillazioni, riportate in regime turbolento, sembra che non siano state riportate con estensione in regime laminare, escluso lo studio di Gelfgat & Gorbunov [72]. In secondo luogo, sembra possibile distinguere, in funzione del parametro S, diversi modelli di struttura del fluido che si modificano fortemente al variare della frequenza, discostandosi considerevolmente dalla struttura a due vortici ben nota in letteratura. Per esempio, mentre per $S = 10$ la tipica struttura di due vortici é chiaramente visibile, all'aumentare della frequenza, cioé $S = 40$, compaiono quattro vortici, due vortici primari e due vortici secondari. In terzo luogo, come in realtá giá notato da Bednarz [15], sembra chiaro che la struttura del fluido evolve nel tempo, portando alla creazione e alla soppressione dei vortici.

Dal punto di vista dell'interpretazione dei fenomeni registrati, al momento non esistono delle spiegazioni totalmente soddisfacenti: innanzitutto non risulta chiaro per quale motivo una distribuzione simmetrica delle forze di Lorentz causi tali asimmetrie nella struttura del fluido. Inoltre, se la dipendenza dalla frequenza della struttura del fluido é giá stata notata da vari autori, come Taberlet & Fautrelle [20], non esistono delle spiegazioni totalmente convincenti sulla radicale differenza dei diversi modelli convettivi al variare della frequenza, se non a livello estremamente qualitativo. Tuttavia, grazie ad una simulazione numerica compiuta tramite OPENFOAM, é stato possibile perlomeno intuire quali potrebbero essere le cause delle oscillazioni: infatti, la simulazione dimostra come il moto del fluido, esclusa una primissima fase, dove la struttura a doppio vortice risulta confermata, si muove poi verso una condizione di moto caotico; questo molto probabilmente é dovuto alla natura tridimensionale del moto del fluido, giá rilevata in regime turbolento da vari autori, come Umbrasko et al. [66] e Bojarevics et al. [67].

Per concludere, risulta provata la possibilitá di condurre ricerche in queste condizioni fisiche, conferma necessaria per procedere verso la seconda fase sperimentale sullo studio delle forze di Leenov-Kolin: inoltre, sorprendentemente alcune nuove osservazioni sono state rilevate che, al meglio delle conoscenze dello scrivente, non sono mai state riportate da studi precedenti. La fase successiva dovrá proseguire nell'indagine della struttura del fluido per capire effettivamente entro quali limiti

sono applicabili le suddette forze di separazione. In particolare, dato che il presente esperimento aveva fin dall'inizio alcune limitazioni, che non hanno permesso di raggiungere frequenze elevate, parrebbe interessante proseguire la ricerca aumentando la frequenza applicata: infatti allo stato attuale delle ricerche, per il massimo S applicato (200), si nota come l'energia cinetica sia ancora troppa elevata per garantire un'efficace applicazione delle forze di Leenov-Kolin. Oltre a ció, la seconda fase dell'esperimento dovrá proseguire le indagini sulla struttura tridimensionale del fluido, ormai provata, installando dei sensori che permettano di rilevare come evolvono i vortici.

BIBLIOGRAPHY

[1] FARADAY, M.: "AN ANALYSIS OF WOOTZ OR INDIAN STEEL." *Quarterly Journal of Science, Literature, and the Arts* **7** (1819) 319–330.

[2] DAVIDSON, P.A.: "AN INTRODUCTION TO MAGNETOHYDRODYNAMICS." *Cambridge University Press* (2001).

[3] HEAVISIDE, O.: "THE INDUCTION OF CURRENTS IN CORES." *Electrician* **12** (1884) 583.

[4] THOMPSON, J. J: "ON THE HEAT PRODUCED BY EDDY CURRENTS IN AN IRON PLATE EXPOSED TO AN ALTERNATING MAGNETIC FIELD." *Electrician* **28** (1882) 599–600.

[5] DE FERRANTI, S. Z.: "PIONEER OF ELECTRIC POWER TRANSMISSION: AN ACCOUNT OF SOME OF THE EARLY WORK OF SEBASTIAN ZIANI DE FERRANTI." *Notes and Records of the Royal Society of London* **19** (1964) 33–41.

[6] NORTHRUP, E. F.: "PRINCIPLES OF INDUCTION HEATING WITH HIGH FREQUENCY CURRENTS." *Transactions of the American Electrochemichal Society* **35** (1919) 69–159.

[7] DAVIDSON, P.A.: "MAGNETOHYDRODYNAMICS IN MATERIALS PROCESSING." *Annu. Rev. Fluid Mech.* **31** (1999) 273–300.

[8] TARAPORE, E. D., EVANS, J. W.: "FLUID VELOCITIES IN INDUCTION MELTING FURNACES: PART I. THEORY AND LABORATORY EXPERIMENTS." *Metall. Trans. B* **7** (1976) 343–348.

[9] LUPI, S. "APPUNTI DI ELETTROTERMIA." *Libreria Progetto* (2005) 325-326.

[10] FAUTRELLE, Y.: "FLUID FLOWS INDUCED BY ALTERNATING MAGNETIC CURRENT." In Lielpeteris, J., Moreau, R. (Eds.):*Liquid Metal Magnetohydrodynamics* (1989) 223–232.

[11] FAUTRELLE, Y.: "ANALYTICAL AND NUMERICAL ASPECTS OF THE ELECTROMAGNETIC STIRRING INDUCED BY ALTERNATING MAGNETIC FIELDS." *J. Fluid Mech.* **102** (1981) 405–430.

[12] GRANDJEAN, P. *Thesis, University of Paris* (1948).

[13] DAMASKOS, N. J.: "THE MAGNETOHYDRODYNAMICS OF THE CORELESS INDUCTION FURNACE." *Ph.D. thesis, Carnegie Mellon University* (1963).

[14] MACANLIS, D.H.: "ELECTROMAGNETIC STIRRING IN THE CORELESS INDUCTION FURNACE." *Ph.D. thesis, Carnegie Mellon University* (1966).

[15] BEDNARZ, T. K.: "AN EXPERIMENTAL INVESTIGATION OF ELECTROMAGNETIC STIRRING IN A CORELESS INDUCTION FURNACE." *Ph.D. thesis, Carnegie Mellon University* (1970).

[16] J. C. R, M., R.,MAXEY: "ESTIMATING VELOCITIES AND SHEAR STRESSES IN TURBULENT FLOWS OF LIQUID METALS DRIVEN BY LOW FREQUENCY ELECTROMAGNETIC FIELDS." *MHD-flows and turbulence. II., Israel Universities Press* (1980) 249–269.

[17] MOREAU, R.: "PROCEEDINGS 2ND BAT-SHEVA SEMINAR IN M.H.D FLOWS AND TURBULENCE." *Israel University Press* (1980).

[18] MOORE, D., J., HUNT, J. C. R.: "PROC. 3RD BAR SHEVA SEMINAR ON LIQUID METAL FLOW AND MAGNETOHYDRODYNAMICS." *Prog. Astro. Aero* **84** AIAA (1982).

[19] TRAKAS, C., TABELING, P., CHABRERIE, J.P.: "ETUDE EXPERIMENTALE DU BRASSAGE TURBULENT DANS LE FOUR A INDUCTION." *Journal de Mécanique Théorique et Appliqué* (1984) 349–370.

Bibliography

[20] TABERLET, E., FAUTRELLE, Y.: "TURBULENT STIRRING IN AN EXPERIMENTAL IN-
DUCTION FURNACE." *J. Fluid Mech.* **159** (1985) 409–431.

[21] CREMER, P., ALEMANY, A.: "ASPECTS EXPÉRIMENTEAUX DU BRASSAGE ÉLEC-
TROMAGNÉTIQUE EN CREUSET." *Journal de Mécanique appliqué* **5** (1981) 37–50.

[22] KOANDA, S., FAUTRELLE Y.R.: "MODELLING OF CORELESS INDUCTION FUR-
NACES: SOME THEORETICAL AND EXPERIMENTAL RESULTS." *Proc. IUTAM Symp.
of Metallurgical Application of MHD (1982), Cambridge, UK* (1984).

[23] LILLICRAP, D. C., MOORE, D., J.: "ELECTROMAGNETIC STIRRING IN CORELESS
INDUCTION FURNACES." *Electroheat for Metals* **3** (1982).

[24] EL-KADDAH, N., SKEZELY, J.: "THE TURBULENT RECIRCULATING FLOW FIELD
IN A CORELESS INDUCTION FURNACE, A COMPARISON OF THEORETICAL PREDIC-
TIONS WITH MEASUREMENTS." *Journal of Fluid Mechanics* **133** (1983) 37–46.

[25] GALPIN, J. M., FAUTRELLE, Y.: "LIQUID METAL FLOWS INDUCED BY LOW-
FREQUENCY ALTERNATING MAGNETIC FIELDS." *Journal of Fluid Mechanics* **239**
(1992) 383–408.

[26] STELIAN, C., VIZMAN, D: "NUMERICAL MODELLING OF FREQUENCY INFLUENCE
ON THE ELECTROMAGNETIC STIRRING OF SEMICONDUCTOR MELTS." *Cryst. Res.
Technol.* **41**:7 (2006) 642–652.

[27] HAMAKI, S. SEYEDEIN, S. H., AFSHAR MOGHADAM, M. R., GHASEMZADEH, R.:
"NUMERICAL SIMULATION OF ELECTROMAGNETIC STIRRING EFFECT ON FLOW PAT-
TERN OF METAL MELT." *Advanced Materials Research* ©Trans. Tec. Publications
(2011) **264-265** 1574–1579.

[28] DUGHIERO, F., FORZAN, M., CISCATO, D.: "A NEW DSS FURNACE FOR ENERGY
SAVING IN THE PRODUCTION OF MULTI CRYSTALLINE SILICON." *Proc. 35th IEEE
Photovoltaic Specialists Conference*, Honolulu, USA (2010) 2165–2170.

[29] CISCATO, D., DUGHIERO, F. ,FORZAN, M: "A COMPARISON BETWEEN RESISTANCE
AND INDUCTION DSS FURNACES FOR SOGSI PRODUCTION." *Proc. EPM* Dresden
(2009)

[30] "SILICON KERF LOSS RECYCLING." *http://www.sikelor.eu*.

[31] LEENOV, D. KOLIN, A.: "THEORY OF ELECTROMAGNETOPHORESIS. I. MAGNETO-
HYDRODYNAMICS FORCES EXPERIENCED BY SPHERICAL AND SYMMETRICALLY
ORIENTED CYLINDRICAL PARTICLES." *J. Chem. Phys.* **22** (1954) 683–688.

[32] MARTY, P.ALEMANY A.: "METALLURGICAL APPLICATIONS OF MAGNETOHYDRO-
DYNAMICS." *Proceedings of the Symposium of IUTAM, Metal Society London* (1984)
245–259.

[33] MAKAROV, S., LUDWIG, R., APELIAN, D.: "ELECTROMAGNETIC SEPARATION
TECHNIQUES IN METAL CASTING. I. CONVENTIONAL METHODS." *IEEE T. Magn.*
40 (2000) 2015–2021.

[34] TANIGUCHI, S. YOSHIKAWA, N., TAKAHASHI, K.: "APPLICATION OF EPM TO THE
SEPARATION OF INCLUSION PARTICLES FROM LIQUID METAL." *Proc. 15th and 6th
Conference on Fundamental and Applied MHD* Riga, 2005 55–63.

[35] KADKHOBAEIGI, M. SAFARIAN, J. TVEIT, H. TANGSTAD, M. JOHANSEN, S. T.:
"REMOVAL OF SIC PARTICLES FROM SOLAR GRADE SILICON MELTS BY IMPOSI-
TION OF HIGH FREQUENCY MAGNETIC FIELD." Trans. Nonferrous Met. Soc. China **22**
(2012) 2813–2821.

[36] CRAMER, A., GALINDO, V.: "FREQUENCY DEPENDENCE OF AN ALTERNATING
MAGNETIC FIELD DRIVEN FLOW." *Proc. Int. Sci. Coll. Modelling for Electromagnetic
Processing* Hannover, Germany (2014).

[37] SHATROV, V., GERBETH, G., HERMANN, R.: "LINEAR STABILITY OF AN
ALTERNATING-MAGNETIC-FIELD-DRIVEN FLOW IN A SPINNING CYLINDRICAL CON-
TAINER." *Physical Review E* **77**:046307 (2008) 1–12.

[38] SHATROV, V., GERBETH, G., HERMANN, R.: "AN ALTERNATING MAGNETIC FIELD DRIVEN FLOW IN A SPINNING CYLINDRICAL CONTAINER." *Journal of Fluids Engineering* **130**:071201 (2008) 1–10.

[39] CRAMER, A., GALINDO, V., ZENNARO, M.: "FREQUENCY DEPENDENCE OF AN ALTERNATING MAGNETIC FIELD DRIVEN FLOW." *Magnetohydrodynamics* **51** 133-147 (2015).

[40] CRAMER, A., GALINDO, V., ZENNARO, M., ECKERT, S.: "INVESTIGATION OF THE FLOW DRIVEN BY AN ALTERNATING MAGNETIC FIELD." *Conference: 8. International Conference on Electromagnetic Processing of Materials* Cannes, France (2015), submitted

[41] MOREAU, R.: "MAGNETOHYDRYNAMICS" *Kluwer Academic Publishers* (1990).

[42] FEYNMAN, R. P., LEIGHTON, B. R., SANDS, M: "THE FEYNMAN LECTURES ON PHYSICS" *Addison Wesley Publishing Company, Inc.* **2** (1964).

[43] LANDAU, L. D., LIFSHITZ, E. M: "ELECTRODYNAMICS OF CONTINUOUS MEDIA (VOLUME 8 OF A COURSE OF THEORETICAL PHYSICS)" *Pergamon Press* (1960).

[44] ROBERTS, P., H.: "AN INTRODUCTION TO MAGNETOHYDRODYNAMICS" *Longmans* (1967).

[45] LANDAU, L. D., LIFSHITZ, E. M: "THE CLASSICAL THEORY OF FIELDS (VOLUME 2 OF A COURSE OF THEORETICAL PHYSICS)" *Buttenworth-Heinemann* (1980).

[46] COHEN, M. I, KUNDU, P. K: "FLUID MECHANICS" *Elsevier Academic Press* (2004).

[47] ACHESON, D. J.: "ELEMENTARY FLUID DYNAMICS" *Oxford University Press* (1990).

[48] METAXAS, A. C.: FOUNDATIONS OF ELECTROHEAT: A UNIFIED APPROACH *John Wiley & Sons Ltd* 1996.

[49] ROHRER MESS- & SYSTEMTECHNIK, MÜNCHEN, GERMANY
`http://www.rohrer-muenchen.de/DE/anwendungen`.

[50] KEYSIGHT TECHNOLOGIES, USA
`http://www.keysight.com`.

[51] SIGNAL PROCESSING, SWITZERLAND
`http://www.signalprocessing.com`.

[52] TAKEDA, Y.: "DEVELOPMENT OF AN ULTRASOUND VELOCITY PROFILE MONITOR." *Nucl. Eng. Design* **126** (1990) 277–284.

[53] TAKEDA, Y.: "VELOCITY PROFILE MEASUREMENTS BY ULTRASONIC DOPPLER METHOD." *Exp. Therm. Fluid Sci.* **10**:4 (1995) 444–453.

[54] TAKEDA, Y.: "MEASUREMENT OF VELOCITY PROFILE OF MERCURY FLOW BY ULTRASOUND DOPPLER SHIFT METHOD." *Nucl Technol* **79** (1987) 120–124.

[55] TAKEDA, Y.: "ULTRASONIC DOPPLER METHOD FOR VELOCITY PROFILE MEASUREMENT IN FLUID DYNAMICS AND FLUID ENGINEERING." *Exp. Fluids* **26** (1999) 177–178.

[56] BRITO, D., NATAF, H.,C., CARDIN, P., AUBERT, J., MASSON, J.P.: "ULTRASONIC DOPPLER VELOCIMETRY IN LIQUID GALLIUM." *Exp. Fluids* **31** (2001) 653–663.

[57] ECKERT, S.,GERBETH, G.: "VELOCITY MEASUREMENT IN LIQUID SODIUM BY MEANS OF ULTRASOUND DOPPLER VELOCIMETRY." *Exp. Fluids* **32** (2002) 542–546.

[58] ECKERT, S., CRAMER, A., GERBETH, G.: "VELOCITY MEASUREMENT TECHNIQUES FOR LIQUID METAL FLOWS." In Molokov, S. et al. (Eds.):*Magnetohydrodynamics- Historical Evolution and Trends* (2007) ©Springer 275-294.

[59] CRAMER, A., ZHANG, C., ECKERT, S.: "LOCAL FLOW STRUCTURES IN LIQUID METALS MEASURED BY AN ULTRASONIC DOPPLER VELOCIMETRY." *Flow Meas. Instrum* **15** (2004) 145–153.

[60] ECKERT, S.,GERBETH, G.,MELNIKOV, V.I.: "VELOCITY MEASUREMENTS AT HIGH TEMPERATURE BY ULTRASOUND DOPPLER VELOCIMETRY USING AN ACOUSTIC WAVE GUIDE." *Exp. Fluids* **35** (2003) 381-388.

[61] ECKERT, S., GERBETH, G., GUNDRUM, T., STEFANI, F.: "VELOCITY MEASUREMENTS IN METALLIC MELTS." *Proc. of 2005 ASME FED Summer Meeting* (2005) FEDSM2005-77089.

[62] RÄBIGER, D., ECKERT, S., GERBETH, G: "MEASUREMENTS OF AN UNSTEADY LIQUID METAL FLOW DURING SPIN-UP DRIVEN BY A ROTATING MAGNETIC FIELD." *Exp. Fluids* **48** (2010) 233–244.

[63] TARAPORE, E. D. , EVANS J. V., LANGFELT, J.: "FLUID VELOCITIES IN INDUCTION MELTING FURNACES. PART II. LARGE SCALE MEASUREMENTS AND PREDICTIONS." *Metallurgical Transactions B* **8 B** (1977) 179–184.

[64] DAVIDSON,P. A., HUNT, J., C., R., MOROS, A.: "TURBULENT RECIRCULATING FLOWS IN LIQUID METAL MHD." *American Institute of Aeronautics and Astronautics, Inc.* (1988) 400-415.

[65] BATCHELOR, G. K.: "ON STEADY LAMINAR FLOW WITH CLOSED STREAMLINES AT LARGE REYNOLDS NUMBER." *Journal of Fluid Mechanics* **1** (1956) 177–190.

[66] UMBRASKO, A., BAAKE, E., NACKE, B., JAKOVICS, A.: "LES-MODELLING AND EXPERIMENTAL INVESTIGATION OF THE MELT FLOW IN INDUCTION FURNACES." *Proc. Int. Sci. Coll. Modelling for Electromagnetic Processing* Hannover, Germany (2003) 2011–2016.

[67] BOJAREVICS, A., BOJAREVICS, V., GELFGAT, Y., PERICLEOUS K.: "LIQUID METAL TURBULENT FLOW DYNAMICS IN A CYLINDRICAL CONTAINER WITH FREE SURFACE: EXPERIMENT AND NUMERICAL ANALYSIS." *Magnetohydrodynamics* **35**:3 (1999) 258–277.

[68] DUGHIERO, F.,FORZAN, M.,POZZA, C.,TOLOMIO, A.: "EXPERIMENTAL RESULTS IN INDUSTRIAL ENVIRONMENT OF THE I-DSS FURNACE." *Proc. Int. Sci. Coll. Modelling for Electromagnetic Processing* Hannover, Germany (2014).

[69] MOFFATT, H. K: "ELECTROMAGNETIC STIRRING." *Physics of Fluids A: Fluid Dynamics* **3** (1991) 1336-1343.

[70] TIR, L., L.: "FEATURES OF MECHANICAL ENERGY TRANSFER TO A CLOSED METAL CIRCUIT IN ELECTROMAGNETIC SYSTEMS WITH AZIMUTHAL CURRENTS." *Magnetohydrodynamics* **12**:2 (1976) 100–108.

[71] UNGARISH, M.: "THE SPIN UP OF A LIQUID METAL DRIVEN BY A ROTATING MAGNETIC FIELD." *Journal of Fluid Mechanics* **347** (1997) 105–118.

[72] GELFGAT, Y., M., GORBUNOV, L., A.: "EFFECT OF ALTERNATING MAGNETIC FIELD ON MELT HYDRODYNAMICS IN A CYLINDRICAL VESSEL WITH A FREE SURFACE." *Magnetohydrodynamics* **30** (1994) 237–247.

[73] BAAKE, E., NACKE, B., JAKOVIČS A., UMBRASKO, A.: "HEAT AND MASS TRANSFER IN TURBULENT FLOWS WITH SEVERAL RECIRCULATED FLOW EDDIES." *Magnetohydrodynamics* **37**:1-2 (2001) 13–22.

[74] BAAKE, E., NACKE, B., UMBRASKO, A., JAKOVIČS, A.: "LARGE EDDY SIMULATION MODELLING OF HEAT AND MASS TRANSFER IN TURBULENT RECIRCULATED FLOWS." *Magnetohydrodynamics* **39**: 3 (2003) 291–297.

[75] UMBRASKO, A., BAAKE, E., NACKE, B. JAKOVIČS, A.: "MODELING OF THE TURBULENT FLOW IN INDUCTION FURNACES." *Metall. Mater. Trans B* **37** (2006) 831–838.

[76] KIRPO, A.,JAKOVIČS, A., BAAKE, E., NACKE, B.: "ANALYSIS OF EXPERIMENTAL AND SIMULATION DATA FOR LIQUID METAL FLOW IN A CYLINDRICAL VESSEL." *Magnetohydrodynamics* **43**:2 (2007) 161–172.

[77] ŠČEPANSKIS M., JAKOVIČS, A., BAAKE, E., NACKE, B.: "ANALYSIS OF THE OSCILLATING BEHAVIOUR OF SOLID INCLUSIONS IN THE INDUCTION CRUCIBLE FURNACE." *Magnetohydrodynamics* **48**:4 (2012) 677–686.

[78] JEONG, J., HUSSAIN F.,: "ON THE IDENTIFICATION OF A VORTEX." *Journal of Fluid Mechanics* **285** (1998) 69–94.